HHS Public Access

Author manuscript

Dev Biol. Author manuscript; available in PMC 2021 August 15.

Published in final edited form as:

Dev Biol. 2020 August 15; 464(2): 161–175. doi:10.1016/j.ydbio.2020.05.010.

Deletion of the *Dishevelled* Family of Genes Disrupts Anterior-Posterior Axis Specification and Selectively Prevents Mesoderm Differentiation

Justine Ngo[1], **Masakazu Hashimoto**[2], **Hiroshi Hamada**[3,4], **Anthony Wynshaw-Boris**[1]

[1]Department of Genetics and Genome Sciences, School of Medicine, Case Western Reserve University, 10900 Euclid Ave, Cleveland, OH, USA.

[2]Laboratory for Embryogenesis, Graduate School of Frontier Bioscience, Osaka University, 1–3 Yamadaoka, Suita, Osaka, Japan 565–0871.

[3]Developmental Genetics Group, Graduate School of Frontier Biosciences, Osaka University, Osaka, Japan.

[4]Laboratory for Organismal Patterning, RIKEN Center for Biosystems Dynamics Research, Kobe, Japan.

Abstract

The Dishevelled proteins transduce both canonical Wnt/β-catenin and non-canonical Wnt/planar cell polarity (PCP) signaling pathways to regulate many key developmental processes during embryogenesis. Here, we disrupt both canonical and non-canonical Wnt pathways by targeting the entire *Dishevelled* family of genes (*Dvl1*, *Dvl2*, and *Dvl3*) to investigate their functional roles in the early embryo. We identified several defects in anterior-posterior axis specification and mesoderm patterning in $Dvl1^{+/-}; Dvl2^{-/-}; Dvl3^{-/-}$ embryos. Homozygous deletions in all three *Dvl* genes (*Dvl* TKO) resulted in defects in distal visceral endoderm migration and a complete failure to induce mesoderm formation. To identify potential mechanisms that lead to the defects in the developmental processes preceding gastrulation, we generated *Dvl* TKO mouse embryonic stem cells (mESCs) and compared the transcriptional profile of these cells with *wild-type* (*WT*) mESCs during germ lineage differentiation into 3D embryoid bodies (EBs). While the *Dvl* TKO mESCs displayed similar morphology, self-renewal properties, and minor transcriptional variation from *WT* mESCs, we identified major transcriptional dysregulation in the *Dvl* TKO EBs during differentiation in a number of genes involved in anterior-posterior pattern specification, gastrulation induction, mesenchyme morphogenesis, and mesoderm-derived tissue development. The absence of the *Dvls* leads to specific down-regulation of BMP signaling genes. Furthermore, exogenous activation of canonical Wnt, BMP, and Nodal signaling all fail to rescue the mesodermal defects in the *Dvl* TKO EBs. Moreover, endoderm differentiation was promoted in the absence of mesoderm in the *Dvl* TKO EBs, while the suppression of ectoderm differentiation was delayed. Overall, we demonstrate that the *Dvls* are dispensable for maintaining self-renewal in

mESCs but are critical during differentiation to regulate key developmental signaling pathways to promote proper axis specification and mesoderm formation.

Introduction

Gastrulation is an essential process in early embryonic development, defined by the differentiation of the pluripotent epiblast into the three definitive germ layers. Before gastrulation induction can proceed, the anterior-posterior (A-P) body axis is specified to properly orient primitive streak formation in the posterior side of the embryo. Wnt signaling is critical for A-P axis specification and helps govern cell fate decision-making during gastrulation by coordinating the expression of Wnt-specific ligands, receptors, and signaling agonists and antagonists (Morkel, 2003; Wang et al., 2012). The complex spatial and temporal expression of Wnt-regulated target genes further intersect with the Bone Morphogenetic Protein (BMP) and Nodal signaling pathways that altogether orchestrate proper embryonic development (Arnold and Robertson, 2009). However, the precise mechanism of how these important pathways interconnect to induce patterning, differentiation, and morphogenesis remains an outstanding question in the field.

The Dishevelled (Dvl) proteins mediate canonical and non-canonical Wnt signaling through specific protein domains (Boutros and Mlodzik, 1999; Wallingford and Habas, 2005). Canonical Wnt signaling is transduced intracellularly by the interaction of the Dvl DIX protein domain with the β-catenin destruction complex, which prevents β-catenin phosphorylation and degradation (Fiedler et al., 2011; Kimelman and Xu, 2006; Kishida et al., 1999; Wallingford and Habas, 2005). The sequestration the β-catenin destruction complex by Dvl results in the stabilization of cytosolic β-catenin that can then enter the nucleus and regulate gene expression as a transcriptional co-factor (Clevers and Nusse, 2012; Nusse and Clevers, 2017). The activation of canonical Wnt signaling is important for the transcriptional regulation of A-P specification and germ lineage differentiation, as mutations in key genes, such as *Wnt3*, *Lrp5/6*, and *β-catenin*, lead to early developmental defects with differing levels of severity (Barrow et al., 2007; Haegel et al., 1995; Huelsken et al., 2000; Kelly et al., 2004; Liu et al., 1999; Robertson et al., 2003; Wang et al., 2012). In *Wnt3* (Barrow et al., 2007; Liu et al., 1999) and *Lrp5/6* (Kelly et al., 2004) mutants, A-P axis specification is properly established, but *β-catenin* mutants completely fail to specify the A-P axis (Haegel et al., 1995; Huelsken et al., 2000). In all of the *Wnt3* (Barrow et al., 2007; Liu et al., 1999), *Lrp5/6* (Kelly et al., 2004), and *β-catenin* (Haegel et al., 1995; Huelsken et al., 2000) null mutants, posterior patterning is severely compromised, and the primitive streak and mesoderm completely fail to form.

The non-canonical Wnt/planar cell polarity (PCP) pathway is β-catenin-independent. Activation of Wnt/PCP is mediated by the Ror2 receptor and its interaction with the Dvl proteins (Ho et al., 2012), via the DEP protein domain (Wallingford and Habas, 2005). Wnt/PCP is essential for several early tissue morphogenesis processes, including cell intercalation during primitive streak formation in chicks (Voiculescu et al., 2007), epithelial-to-mesenchymal transition during A-P axis elongation (Andre et al., 2015), establishing cellular polarity in node cells (Hashimoto et al., 2010), and regulating convergent-extension

movements during neurulation (Vladar et al., 2009; Wang et al., 2006). Deletion of *Prickle1*, a core PCP component, results in the lack of primitive streak and mesoderm formation (Tao et al., 2009), which is reminiscent of the phenotypes observed in canonical Wnt mutants. Since canonical and non-canonical Wnt mutants both develop similar peri-implantation lethal phenotypes, the extent of how much each pathway directly and indirectly contributes to the gastrulation defects remains unclear.

The *Dvl* family of genes (*Dvl1*, *Dvl2*, and *Dvl3*) are broadly expressed and highly conserved. Each *Dvl* gene has unique functions that are developmentally important, as single null mutations lead to distinct phenotypes. $Dvl1^{-/-}$ mutants manifest social behavior deficits (Lijam et al., 1997); $Dvl2^{-/-}$ mutants display defects in heart development, somite segmentation, and neural tube closure (Hamblet et al., 2002); and $Dvl3^{-/-}$ mutants display heart development abnormalities and inner ear stereocilia disorganization (Etheridge et al., 2008). Double *Dvl* mutants develop novel and more severe overlapping phenotypes, including craniorachischisis and axial truncation, suggesting that functional redundancy is present (Etheridge et al., 2008; Hamblet et al., 2002; Wang et al., 2012; Wynshaw-Boris, 2012). Conditional deletion of the *Dvls* in ependymal cells that line the ventricles in the brain of $hGFAP\text{-}Cre; Dvl1^{-/-}; Dvl2^{flox/flox}; Dvl3^{+/-}$ mice lead to hydrocephalus (Ohata et al., 2014). Decreasing the gene dosage of the *Dvls* leads to increased severity of developmental phenotypes, such as in $Dvl1^{-/-}; Dvl2^{-/-}; Dvl3^{+/-}$ embryos that develop disorganized nodal cilia (Hashimoto et al., 2010). With the exception of the social behavior abnormalities, which are attributed to canonical Wnt pathway deficits (Belinson et al., 2016), the somite segmentation, neural tube defects, and disorganization of stereocilia and nodal cilia are primarily associated with the functions of Wnt/PCP signaling.

The importance of both Wnt signaling pathways on embryonic development is evident based on the severe morphogenetic defects that arise in canonical Wnt and PCP mutants. However, the redundancy of Wnt signaling components has made suppressing both Wnt pathways genetically *in vivo* a major challenge, especially when perturbing these pathways lead to peri-implantation lethality. In this study, we disrupted the entire *Dvl* family of genes to generate *Dvl* triple mutant embryo and cellular models to determine how decreasing *Dvl* gene dosage impacts pre- and post-implantation developmental processes. Overall, we demonstrate that the *Dvls* are dispensable for maintaining self-renewal, but are required for proper axis specification, and mesoderm formation and maintenance during differentiation. Furthermore, we systematically test whether activating canonical Wnt, BMP and Nodal signaling could rescue mesodermal differentiation *in vitro* in *Dvl* triple knockout (TKO) mutants. While activation of these pathways failed to promote and maintain mesoderm differentiation, we found that BMP and Wnt inhibition enhanced endoderm differentiation in the absence of the *Dvls*.

Experimental Details

Generation of *Dishevelled* Mutant Mice

All animal care and experimental procedures were conducted in accordance to the protocol approved by the Institutional Animal Care and Use Committee at Case Western Reserve University. To generate *Dvl* mutant embryos, $Dvl1^{+/-}; Dvl2^{-/-}; Dvl3^{+/-}$ mice were back-

crossed (as double knockout mutants are gestational lethal) to produce *Dvl1*$^{+/-}$; *Dvl2*$^{-/-}$; *Dvl3*$^{-/-}$ and *Dvl1*$^{-/-}$; *Dvl2*$^{-/-}$; *Dvl3*$^{-/-}$ embryos. *Dvl1*$^{-/-}$; *Dvl2*$^{+/-}$; *Dvl*$^{+/-}$ were crossed to produce *Dvl1*$^{-/-}$; *Dvl3*$^{+/-}$, *Dvl1*$^{-/-}$; *Dvl3*$^{-/-}$, and *Dvl1*$^{-/-}$; *Dvl2*$^{-/-}$; *Dvl3*$^{-/-}$ embryos. *WT* embryos expressing *Dvl2-EGFP* and *Dvl3-EYFP* BAC alleles were generated by crossing mice previously described in Wang et al. (2006).

Genotyping analyses were performed by PCR using genomic DNA from tail tips or whole embryos post-staining. The primer combinations were previously described and used to genotype *Dvl1* (Lijam et al., 1997), *Dvl2* (Hamblet et al., 2002; Ohata et al., 2014) and *Dvl3* (Etheridge et al., 2008).

Whole-Mount *In Situ* Hybridization and Embryo Immunostaining

Whole-mount *in situ* hybridization with specific probes for Brachyury was performed on E7.5 embryos according to standard protocols. Immunostaining of E6.5 embryos were dissected and immunostained according to Hashimoto et al. (2010).

Derivation, Culture, and Maintenance of *Dishevelled* Mutant Mouse Embryonic Stem Cells

Male and female *Dvl1*$^{-/-}$; *Dvl2*$^{flox/flox}$; *Dvl3*$^{+/-}$ mice (Ohata et al., 2014) were mated to produce *Dvl1*$^{-/-}$; *Dvl2*$^{flox/flox}$; *Dvl3*$^{-/-}$ (*Dvl* DKO) blastocysts. Timed matings were performed to obtain blastocysts at E3.5 as previously described (Bryja et al., 2006). *Wild-type* (*WT*) blastocysts were isolated similarly as the *Dvl* mutants. Each blastocyst was placed in a separate well of a 0.1% porcine gelatin-coated 4-well plate with a feeder layer of mitotically inactivated mouse embryonic fibroblasts (iMEFs). The blastocysts and derived mESC lines were cultured in Iscove's Modified Dulbecco's Medium (IMDM) supplemented with 1×10^6 units of LIF (EMD Millipore), 20% knockout serum replacement (KOSR), 1% nonessential amino acids, 1% GlutaMAX, 1% penicillin/streptomycin, and β-mercaptoethanol. Fresh media containing LIF was replenished daily. By day 3, the blastocysts attached onto the plate and began to hatch, forming a single outgrowth from the inner cell mass. On day 6, each outgrowth was manually picked and dissociated into small clusters of cells with 0.05% trypsin. The trypsin was inactivated with FBS-containing medium, and cells were plated back into a single well of a 4-well plate on a new layer of iMEFs. Multiple colonies appeared by day 11 and were passaged using 0.05% trypsin for further expansion. The mESC lines were continued to be fed daily with fresh LIF and passaged every 3 days (Zhang et al., 2018). To minimize iMEF contamination, the mESC colonies were incubated for 15 minutes at 37°C with a 1 ml mixture of 1 mg/ml collagenase IV (Thermo Fisher Scientific) and 1 mg/ml dispase (Thermo Fisher Scientific) dissolved in IMDM. Intact colonies were pelleted for 15 seconds followed by a PBS wash. This brief pelleting and wash process was repeated 3 times to remove single cell iMEFs. Genomic DNA was isolated for genotyping by PCR using the DNeasy Blood and Tissue kit (Qiagen) according to the manufacturer's instructions. The primers described in Supplemental Table S1 were used for genotyping mESCs.

Generation of *Dvl1*$^{-/-}$; *Dvl2*$^{-/-}$; *Dvl3*$^{-/-}$ (*Dvl* TKO) mESCs

Transfection of *Dvl1*$^{-/-}$; *Dvl2*$^{flox/flox}$; *Dvl3*$^{-/-}$ mESCs with the Cre-IRES-PuroR plasmid (Addgene #30205) was carried out using the Fugene HD Transfection Reagent (Promega)

according to the manufacturer's instructions. After 48 h post-transfection, the positive mESC clones were selected by 2.0 μM puromycin (Thermo Fisher Scientific) treatment for 1 week. PCR primers flanking the loxP sites in intron 1 and exon 15 of *Dvl2* were used to detect deletion after Cre recombination. The C/F primers amplifies the wild-type (337 bp) and floxed (441 bp) region of intron 1, and the G/J primers amplifies the wild-type (450 bp) and floxed (550 bp) region of exon 15 (Supplemental Figure 1A) (Ohata et al., 2014). A combination of the C/G/J primers were used to detect *Dvl2* deletion. In the event of recombination, the C (intron 1) and J (exon 15) primers amplified a 393 bp "deleted" band, while the 550 bp "floxed" band produced by the G and J primers were no longer amplified. Only the 450 bp band would be present in *WT*. The C/F/J combination of primers were tested, but the sizes of the resulting "floxed" 441 bp and 393 bp "deleted" bands were more difficult to resolve (data not shown). Additional primers for exon 5–7 in *Dvl2* were used to confirm deletion. *Dvl1* and *Dvl3* deletion were confirmed in the *Dvl* TKO mESCs. All genotyping primers are described in Supplemental Table S1.

RNA-Sequencing and Gene Expression Analysis

RNA was extracted with TRIzol Reagent (Thermo Fisher Scientific) from mESCs and embryoid bodies that were cultured for 7 days. RNA purification was performed using the Direct-zol RNA Mini-Prep kit (Zymo Research). RNA libraries for each sample were prepared using the Illumina TruSeq Stranded Total RNA Library Prep Kit according to the manufacturer's instructions, and sequenced on the Illumina HiSeq 2500 system in rapid run mode at the Case Western Reserve University Genomics Core Facility. Raw paired-end 100 bp reads were trimmed and filtered using cutadapt (options: −q 20 −m 25) (Martin, 2011). Quality reads were aligned to mm10 using HISAT2 (Kim et al., 2015; Pertea et al., 2016) and converted to sorted BAM files using samtools (Li et al., 2009). Identification of differentially expressed genes using DESeq2 (Love et al., 2014), principal component analysis (PCA), and additional statistical analyses were performed in R (version 3.5.3). Gene set enrichment analysis (GSEA) was performed as described in Subramanian et al. (2005). Gene ontology analysis was performed using the online Gene Ontology Consortium resource (Ashburner et al., 2000).

Embryoid Body Formation and Drug Treatment

Prior to embryoid body formation, all mouse ESCs were maintained on 0.1% porcine gelatin without a feeder layer for at least 2 passages to minimize residual iMEF contamination. The mESCs were passaged into single cells, quantified using the Countess II Automated Cell Counter (Thermo Fisher Scientific), and 10,000 cells were seeded per well into a 96-well low attachment V-bottom plate (Sumitomo). The cells were cultured in IMDM supplemented with 20% FBS, 1% nonessential amino acids, 1% GlutaMAX, 1% penicillin/streptomycin, and β-mercaptoethanol. The following drug treatments were added at the time of plating and removed after 48 hours: 100 ng/ml Activin A (R&D Systems), 50 ng/ml BMP4 (R&D Systems), 3uM CHIR-99021 (Tocris), 100 ng/ml Wnt3a (R&D Systems), 10 uM SB-431542 (EMD Millipore), 200 nM LDN-193189 (Stemgent), 0.5 uM IWP L6 (Tocris). Non-adherent embryoid bodies aggregated within 2 days in culture. The media was changed on days 2 and 6. EBs were collected on days 2–7 for DNA, RNA, and protein extraction, and immunostaining.

Gene Expression Analysis by Quantitative RT-PCR

Total RNA from the embryoid bodies cultured for 2–6 days was extracted using TRIzol Reagent (Thermo Fisher Scientific) followed by purification with the Direct-zol RNA Mini-Prep kit (Zymo Research). RNA concentration was measured using the NanoDrop 1000. The Superscript IV First Strand Synthesis Master Mix (Thermo Fisher Scientific) was used according to the manufacturer's instructions to reverse transcribe 200 ng of each sample for complementary DNA synthesis. The cDNA was diluted at a ratio of 1:3 in DNase/RNase-free water, and 0.5 μl was used for PCR amplification with the POWER Up SYBR Green PCR Master Mix (Thermo Fisher Scientific). The primers used were previously described in Zhang et al. (2018) and Kurokawa et al. (2004). Real-time detection of mRNA expression was performed with the Life Technologies QuantStudio™ 12 K Flex Real-Time PCR System. Every reaction was carried out in quadruplicate, and the fold changes were calculated using the comparative Ct method previously described (Schmittgen and Livak, 2008; Willems et al., 2008). The resulting Ct values were normalized to β-actin at the earliest time-point in the control wild-type embryoid bodies. Results are shown ± SEM of the mean of at least three independent experiments.

Immunofluorescence Staining

For adherent cell immunofluorescence staining, the cells were washed in PBS, fixed with 4% paraformaldehyde in PBS for 15 min at room temperature, washed for 5 min 3 times with PBS, and permeabilized with 0.5% Triton X-100 in PBS for 10 min. Blocking was performed with 10% donkey serum in PBS for at least 1 h, followed by overnight primary antibody incubation at 4°C. The following primary antibodies were diluted in the blocking solution: Sox2 (Abcam, 1:500) and Oct4 (Santa Cruz; 1:400). Following three 5 min washes in PBS, the cells were incubated with the appropriate secondary antibodies conjugated with Alexa Fluor 488 or Alexa Fluor 555 (Thermo Fisher Scientific; 1:500) for 30 min at room temperature. Cells were counterstained with DAPI (Sigma Aldrich, 1:2000) for 5 min. Fluorescence was visualized with the Leica DM6000 inverted microscope. Images were acquired using the Q-Imaging Retiga Xi Firewire High-Speed, 12-bit cooled CCD camera and Volocity software.

For embryoid body immunofluorescence staining, the EBs were washed once in PBS, fixed with 4% paraformaldehyde/PBS overnight at 4°C, followed by three 5 min PBS washes. The EBs were cryopreserved in 30% sucrose overnight at 4°C, transferred to a 1:1 mixture of 30% sucrose and OCT (Thermo Fisher Scientific), and frozen in 100% OCT. Frozen 20 μm thick sections were allowed to equilibrate at room temperature for 10 min, and the OCT was removed with TBS. The EB sections were permeabilized with TBS-0.5% Triton X-100 for 12 min and blocked for at least 1 h in 10% donkey serum, 1% filtered bovine serum albumin (Sigma Aldrich), and 1% fish gelatin (Sigma Aldrich) in TBS-0.1% Triton X-100 (TBS-T). Brachyury (abcam; 1:200) and Otx2 (Neuromics; 1:200) antibodies were diluted in the blocking solution and incubated overnight at 4°C. Following three 10 min washes in TBS-T, the appropriate secondary antibodies conjugated with Alexa Fluor 488 or Alexa Fluor 555 (Thermo Fisher Scientific; 1:500) were incubated for 30 min at room temperature. The nuclei were counterstained with DAPI (1:2000) for 5 min. Images were acquired with the Hamamatsu S60 Slide Scanner. Quantification of cell counts and EB areas was performed

using the Visiopharm software and R (version 3.5.3). The R script for measuring EB area can be found at https://github.com/geolee123/CellMicroscopyTools.

Western Blotting

Mouse ESCs were washed with ice-cold PBS, scraped, and pelleted. Protein was extracted with 50 mM Tris-HCl pH 8, 150 mM NaCl, 0.5% sodium deoxycholate, 0.1% SDS, 1% Triton X-100, and protease inhibitor cocktail (Sigma Aldrich) and incubated for 30 min at 4°C with shaking. Whole cell lysates were centrifuged for 30 minutes at 15,000 rpm at 4°C, and the supernatant was collected. Protein concentration was measured using the Bradford assay (BioRad). Samples were prepared in NuPAGE LDS sample buffer and reducing agent (Thermo Fisher Scientific) and boiled for 5 min at 95°C. SDS-PAGE was performed with 15 μg of protein, followed by protein transfer to nitrocellulose membranes (Thermo Fisher Scientific). Blocking was performed for at least 1 h with 5% non-fat milk in TBS-T. The following primary antibodies were incubated overnight at 4°C: Dvl2 (Cell Signaling Technologies; 1:1000), Dvl3 (Cell Signaling Technologies; 1:1000), β-actin (Sigma Aldrich; 1:5000). After three 5 min washes with TBS-T, the appropriate secondary antibodies conjugated with HRP (Cell Signaling Technologies, 1:1000) were incubated for 1 h at room temperature. The membranes were visualized using the Pierce ECL Plus Substrate (Thermo Fisher Scientific) and images of the immunoblots were captured with the LI-COR Odyssey Fc.

Statistical Analysis

Significant differentially expressed genes were identified based on a False Discovery Rate adjusted p-value of 0.05. In qRT-PCR experiments, statistical significance among the drug treatments and genotypes was determined using ANOVA with alpha = 0.05. In the cell quantification experiments, Student's unpaired *t* test was used to determine significance between genotypes for each marker. Statistical analyses were performed using GraphPad Prism (version 8.3.0). The mean values are shown with the SEM.

Results

Loss of the Dvls Disrupts Anterior-Posterior Axis Specification and Mesoderm Patterning

In previous studies, we failed to recover *Dvl2*$^{-/-}$*; Dvl3*$^{-/-}$ embryos from litters beyond E8.5 (Wynshaw-Boris, 2012). We hypothesized that these embryos developed defects around the time of gastrulation, so we performed *in situ* hybridization staining at E7.5 for Brachyury, an early mesodermal marker (Kispert and Herrmann, 1994; Yamaguchi et al., 1999). In contrast to *WT*, which displayed restricted Brachyury along the posterior embryo (Figure 1A), Brachyury expression in *Dvl2*$^{-/-}$*; Dvl3*$^{-/-}$ appeared to be widespread throughout the entire embryo due to excessive accumulation of mesodermal tissue in the posterior side of the embryo (Figure 1B).

We next investigated how decreasing the *Dvl* gene dosage would further disrupt mesoderm patterning by generating *Dvl1*$^{+/-}$*; Dvl2*$^{-/-}$*; Dvl3*$^{-/-}$ embryos and observed incomplete penetrance of multiple patterning defects (Figure 1C–1E) at E7.5. A subset of *Dvl1*$^{+/-}$*; Dvl2*$^{-/-}$*; Dvl3*$^{-/-}$ embryos displayed proximal Brachyury expression, indicative of abnormal

A-P axis specification (Figure 1C–C'). In two *Dvl1*$^{+/-}$; *Dvl2*$^{-/-}$; *Dvl3*$^{-/-}$ embryos, the Brachyury-expressing cells clustered in the proximal posterior region, suggesting that the A-P axis was established, but the mesodermal cells were defective in migrating out of the primitive streak (Figure 1D–D'). Another pair of *Dvl1*$^{+/-}$; *Dvl2*$^{-/-}$; *Dvl3*$^{-/-}$ embryos appeared to have disorganized ectoderm and abnormal anterior patterning (Figure 1E–E'). Overall, these results demonstrate that a single *Dvl* allele is sufficient to induce mesoderm formation, but decreasing the dosage of the *Dvls* leads to abnormalities in anterior and posterior patterning as well as defective mesoderm migration out of the primitive streak.

To examine whether mesoderm induction is dependent on functional Dvls, we generated *Dvl1*$^{-/-}$; *Dvl2*$^{-/-}$; *Dvl3*$^{-/-}$ (*Dvl* TKO) embryos. *Dvl1*$^{-/-}$; *Dvl2*$^{+/-}$; *Dvl3*$^{+/-}$ mice were crossed to produce *Dvl* TKO embryos at a Mendelian ratio of 1:16. Litters were typically small, and *Dvl* TKO embryos were peri-implantation lethal. The overall size of stage-matched *Dvl* TKO embryos was smaller than *WT*, *Dvl2*$^{-/-}$; *Dvl3*$^{-/-}$, and *Dvl1*$^{+/-}$; *Dvl2*$^{-/-}$; *Dvl3*$^{-/-}$ embryos. Moreover, *Dvl* TKO embryos lacked Brachyury expression at E7.5 and failed to induce mesoderm differentiation (Figure 1F–1F'). Based on these results, mesoderm induction requires functional Dvl activity.

To test whether the *Dvls* are required for A-P axis specification, we first determined the expression and localization of the Dvls in the distal and anterior visceral endoderm (DVE and AVE) using *WT* embryos ubiquitously expressing *Dvl2-EGFP* or *Dvl3-EYFP* BAC transgenes, which function similarly to endogenous Dvls since they can fully rescue the phenotypes of *Dvl2*$^{-/-}$ and *Dvl3*$^{-/-}$ mice (Etheridge et al., 2008; Wang et al., 2006) and localize to the posterior side of node cells (Hashimoto et al., 2010). In E6.5 *WT* embryos, *Dvl2-EGFP* (Figure 1G) and *Dvl3-EYFP* (Figure 1H) localized in a polarized fashion in the DVE and AVE, suggesting that the Dvls are involved in DVE migration to the prospective anterior during the process of axis specification. Next, we determined whether the *Dvl* mutants properly express Lefty1, which is important in activating DVE migration (Takaoka et al., 2011; Yamamoto et al., 2004). We observed Lefty1 expression in the DVE of *Dvl1*$^{-/-}$; *Dvl3*$^{+/-}$ (Figure 1I) and *Dvl1*$^{-/-}$; *Dvl3*$^{-/-}$ (Figure 1J) E6.5 embryos. However, Lefty1 is absent in the *Dvl* TKO embryos (Figure 1K), resulting in the failure to promote DVE migration to specify the A-P axis. Nodal expression was previously demonstrated to be absent in *Dvl1*$^{-/-}$; *Dvl2*$^{-/-}$; *Dvl3*$^{+/-}$ embryos, so the expression of Lefty1 is not dependent on Dvl2 (Hashimoto et al., 2010).

Altogether, these results support the requirement of the *Dvl* genes to regulate mesoderm formation and DVE migration to establish the A-P axis. We found that decreasing the gene dosage of the *Dvls* results in more severe defects in the overall patterning of the anterior-posterior axis and mesoderm, which suggests the gene redundancy of the *Dvls* may be important for maintaining a critical activity threshold in the embryo.

Loss of the *Dvls* Does Not Negatively Affect the Self-Renewal Properties of Mouse Embryonic Stem Cells

The early lethality and low probability of generating *Dvl* TKO embryos limited our ability to fully assess the A-P axis defects and whether the other germ lineages were properly established. To further investigate the impact of *Dvl* loss on germ lineage differentiation and

define the genes that are dysregulated during axis specification and mesoderm induction, we generated *Dvl* TKO mouse embryonic stem cells (mESCs) and differentiated these cells into 3D spheroid cell aggregates called embryoid bodies (EBs) (Figure 2A), which have been widely used to model germ lineage specification during gastrulation *in vitro* (Biechele et al., 2011; ten Berge et al., 2008; Turner et al., 2017). To obtain *Dvl* TKO mESCs, we isolated and transfected $Dvl1^{-/-}; Dvl2^{flox/flox}; Dvl3^{-/-}$ (*Dvl* DKO) mESCs with EF1α-Cre recombinase (Figure 2A, Supplemental Figure 1A–B) to induce deletion of floxed *Dvl2* (Supplemental Figure 1A, 1D–E, 1G). Deletion of the *Dvl1* and *Dvl3* was confirmed in *Dvl* DKO and TKO mESCs by PCR (Supplemental Figure 1C, 1F) and RNA-seq (data not shown). Furthermore, Dvl2 and Dvl3, which have reliable antibodies available, were not expressed at the protein level in the *Dvl* TKO mESCs (Supplemental Figure 1G).

Absence of the *Dvls* in mESCs did not negatively impact survival and proliferation, as *Dvl* TKO mESCs were cultured stably for over 20 passages. The *Dvl* TKO mESCs express pluripotency markers, Sox2 and Oct4, and their colony morphology were indistinguishable from *WT* mESCs (Figure 2B). Karyotypically, *WT* mESCs were normal (Supplemental Figure 1H). However, *Dvl* DKO (Supplemental Figure 1I) and the derived *Dvl* TKO (Supplemental Figure 1J) mESCs displayed loss of a sex chromosome. This phenomenon has been documented in mouse ES lines (Gaztelumendi and Nogues, 2014; Sugawara et al., 2006), and is not expected to affect germ lineage differentiation, as female mice with a single X chromosome are developmentally normal and fertile (Probst et al., 2008; Russell et al., 1959).

Previous studies have suggested that active canonical Wnt signaling is required to reinforce a state of self-renewal in mESCs (Faunes et al., 2013; Kelly et al., 2011). However, we did not observe obvious morphological differences between *WT* and *Dvl* TKO mESCs to indicate premature differentiation among the *Dvl* TKO mESCs. Therefore, we assessed whether there were major transcriptional differences in *WT* and *Dvl* TKO mESCs and EBs by RNA-seq. Principal component analysis among *WT* and *Dvl* TKO mESCs revealed an average absolute variance of 2.5% and 6.8% along PC1 and PC2, respectively (Figure 2D). The *WT* and *Dvl* TKO EBs that have been differentiating for 7 days (Figure 2C), displayed an average absolute variance of 31.3% along PC2 (Figure 2D), suggesting that the *Dvls* play a larger role during differentiation than during self-renewal. One of the biological replicates for *WT* and *Dvl* TKO mESCs contained some differentiated cells, which led to clustering with the EBs (Figure 2D). We performed genome-wide gene set enrichment analyses (GSEA) on *WT* and *Dvl* TKO mESCs and EBs. There was no significant enrichment of genes for specific biological processes in comparisons among *WT* and *Dvl* TKO mESCs. However, among differentiated *WT* and *Dvl* TKO EBs, we identified an enrichment of genes involved in anterior-posterior pattern specification, mesenchyme morphogenesis, regulation of animal organ formation, and heart morphogenesis (Figure 2E). Overall, our results demonstrate that Dvl-mediated Wnt activity is dispensable for maintaining a state of self-renewal, but is required during differentiation.

Identification of Dysregulated A-P Patterning and Gastrulation-Associated Genes in *Dvl* TKO Embryoid Bodies

A total of 217 differentially expressed (DE) genes were identified (FDR < 0.05) in the mESCs by unsupervised hierarchical clustering (Figure 3A). A majority of these DE genes were unannotated or non-coding genes (Supplemental Table 2). To confirm Cre-mediated deletion of floxed *Dvl2*, we found that *Dvl2* was significantly differentially expressed among *WT* and *Dvl* TKO mESCs (Supplemental Figure 1K). We performed GSEA on the DE genes in mESCs, but found no significant biological process enrichment. A total of 330 DE genes (FDR < 0.05) were identified among differentiated *WT* and *Dvl* TKO EBs, of which, 173 were up-regulated and 157 were down-regulated in *Dvl* TKO (Figure 3B). When we performed GSEA on the DE genes in the EBs, we identified gene enrichment among Wnt signaling, pattern specification, and gastrulation (Figure 3C). Several genes overlapped among the significant biological processes, such as *Mesp1*, *Fgf8*, *Dkk1*, and *Wnt3* (Figure 3C). We were interested in other biological processes represented by the group of 157 down-regulated genes in the *Dvl* TKO EBs, so we performed gene ontology (GO) analysis and observed significant GO terms for Wnt signaling, AP axis and pattern specification, mesoderm, endoderm, and neural plate development, Bone Morphogenetic Pathway (BMP) signaling response, and gastrulation and mesodermal cell migration (Figure 3D). No significant GO terms were identified among the up-regulated genes in the *Dvl* TKO EBs.

We further compared the relative expression of genes in specific GO terms (Figure 3D, bolded) to infer functional activity. First, we assessed whether the canonical and non-canonical Wnt pathways were disrupted in *Dvl* TKO EBs, and observed down-regulation in regulatory and target genes, such as *Axin2*, *Sp5*, *Wnt3*, and *Dkk1* involved in canonical Wnt signaling (Figure 3E) and *Wnt5a*, *Celsr1*, *Vangl2*, and *Ror2* involved in Wnt/PCP signaling (Figure 3F). We examined additional genes that are important in patterning and gastrulation, and identified 81 AP axis specification genes (Figure 3G) and 69 gastrulation induction genes (Figure 3H) that were down-regulated in the *Dvl* TKO EBs. Overall, these results demonstrate that the absence of the *Dvls* disrupts both canonical and non-canonical Wnt signaling during differentiation, and deletion of the *Dvl* family of genes selectively dysregulates a significant number of genes required for axis formation and gastrulation induction.

Loss of the *Dvls* Suppresses Mesoderm Induction but Endoderm and Ectoderm Differentiation Remain Intact

We next examined the genes in the GO terms involved in germ lineage development previously identified in our gene ontology analysis (Figure 3D). We identified 37 genes required for mesoderm formation, some of which are not direct β-catenin targets, that were significantly down-regulated in the *Dvl* TKO EBs (Figure 4A). This result is consistent with the *Dvl* TKO *in vivo* phenotype (Figure 1F). Several endoderm (i.e. *Sox17* and *Gata4*) and neuroectoderm (i.e. *Pax6* and *Otx2*) genes were upregulated in *Dvl* TKO EBs compared to *WT*, demonstrating that induction of these lineages was not completely disrupted in the absence of the *Dvls* (Figure 4B–C). However, despite the upregulation of endodermal and ectodermal lineage identity genes in the *Dvl* TKO EBs, we observed down-regulation of transcription factors that are required for patterning and organization, such as *Hnf1b* and

Dab2 (Figure 4B, for endoderm) as well as *Ptch1*, *Tbx2*, and *Tbx3* (Figure 4C, for ectoderm). Therefore, the maintenance and patterning of these lineages *in vivo* could potentially be abnormal in the *Dvl* TKO EBs after induction.

We performed Brachyury and Otx2 immunostaining at the end of the differentiation process (Figure 4D–E). In *WT* EBs, there was a mean of 16.5% ± 0.03 Brachyury-positive cells, while there were no detectable Brachyury-positive cells in all *Dvl* TKO EBs analyzed (Figure 4E, n=20 EBs/genotype). There was a slightly higher number of Otx2-positive cells in the *Dvl* TKO EBs (51.0%±0.020), compared to *WT* EBs (46.0%±0.025), but this difference was not statistically significant (Figure 4F).

To determine the differences in germ lineage induction throughout the EB differentiation time course, we measured the relative mRNA levels of Brachyury (mesoderm, Figure 4G), GATA4 (endoderm, Figure 4H), and Otx2 (ectoderm, Figure 4I). Brachyury expression increased 32 to 172-fold in *WT* EBs, while remaining at baseline in *Dvl* TKO EBs over time (Figure 4G). While the relative expression levels of GATA4 and Otx2 mRNA in *Dvl* TKO EBs were higher than *WT* EBs throughout the differentiation time course, the fold differences were not statistically significant (Figure 4H–I). Overall, these results demonstrate that the loss of the *Dvls* selectively inhibits mesoderm differentiation, but endoderm and ectoderm differentiation remain intact.

Activation of Canonical Wnt, BMP, and Nodal Signaling Fails to Rescue Mesoderm Differentiation in *Dvl* TKO Embryoid Bodies

Wnt signaling activates BMP and Nodal pathways to coordinate important developmental processes, so we determined whether the absence of Dvl-mediated Wnt signaling negatively impacts the expression of key genes in these pathways. Several BMP-associated genes were down-regulated in the *Dvl* TKO EBs, such as *Bmpr1a*, *Bmp2*, *Bmp4*, *Bmp5*, *Bmp7*, *Smad1* and *Smad4*, all of which have been shown to be required in primitive streak formation (Figure 5A) (Zhao, 2002). Conversely, not all Nodal target genes were down-regulated in the *Dvl* TKO EBs, but we observed decreased expression of Nodal regulatory genes, such as *Cer1*, and genes that mediate Nodal-dependent left-right asymmetry, such as *Cfc1* and *Pkd1l1* (Figure 5B).

We tested whether activating canonical Wnt, BMP, and Nodal signaling could rescue the mesoderm differentiation defects in the *Dvl* TKO EBs. During the first 2 days of EB formation, *WT* and *Dvl* TKO cells were directly stimulated with drug treatment to ensure uniform exposure among the aggregating cells (Supplemental Figure 2A–C). We observed changes in morphology (Supplemental Figure 2B–C) and measured the 2-dimensional area of each EB to infer whether the cells were actively proliferating over the differentiation time course (Supplemental Figure 2D). *WT* EBs displayed increased complexity and larger outgrowths over time, while the overall structure of the *Dvl* TKO EBs remained round with a distinct outer ectodermal ring (Supplemental Figure 2B–C) (Coucouvanis and Martin, 1999). Treatment with BMP (BMP4), canonical Wnt (Wnt3a and CHIR-99021), and Nodal (Activin A) pathway activators all led to increased areas over time in the *WT* EBs relative to the untreated *WT* controls (Supplemental Figure 2B, 2D), demonstrating effective doses of these activators. Compared to the untreated *Dvl* TKO controls, BMP4 and Activin A

treatment resulted in increases in the overall EB areas on days 6–7 of differentiation, but Wnt3a and CHIR-99021 did not significantly increase *Dvl* TKO EB size (Supplemental Figure 2C, 2D).

We next evaluated the effect of each treatment on the differentiation potential of the three germ lineages. *WT* and *Dvl* TKO EBs were treated with Wnt3a and CHIR-99021 to activate canonical Wnt signaling (Figure 5C–D). Wnt3a functions upstream of the Dvl proteins, whereas CHIR-99021 functions downstream of the Dvl proteins to stabilize β-catenin. Compared to the untreated *WT* control, Wnt3a and CHIR-99021 treatment did not appear to enhance the overall number of Brachyury-positive cells in *WT* EBs (Figure 5C, 5E). However, CHIR-99021, but not Wnt3a, treatment resulted in earlier Brachyury induction at day 2 of differentiation, compared to the untreated *WT* control that induced Brachyury by day 4 (Figure 5G). These results suggest that Wnt activation affects the timing of mesoderm induction rather than the expansion of the number of Brachyury-positive mesodermal cells within the EBs.

In the *Dvl* TKO EBs, neither Wnt3a nor CHIR-99021 resulted in the presence of Brachyury-positive cells by IHC (Figure 5D–E). Wnt3a did not rescue Brachyury mRNA expression, while CHIR-99021 treatment appeared to induce Brachyury mRNA expression on day 2 when the EBs were still directly exposed to this drug (Figure 5G). In the absence of direct stimulation by CHIR-99021 in the *Dvl* TKO EBs, we observe that the Brachyury levels returned to baseline and were not maintained over the time course of differentiation (Figure 5G). These results demonstrate that canonical Wnt can be activated in the absence of the Dvls, as CHIR-99021 activates canonical Wnt downstream of the Dvls, but the Dvls are required to maintain Wnt activity to induce mesoderm differentiation.

We next tested whether BMP and Nodal signaling could rescue the mesoderm differentiation defects in *Dvl* TKO EBs independently of Wnt activation. BMP4 and Activin A treatments both led to an increase in the number of Brachyury-positive cells in *WT* EBs (Figure 5C, 5E). BMP4 induced Brachyury expression earlier than the untreated control and Activin A treatment (Figure 5G). Furthermore, BMP4 and Activin A both resulted in more robust Brachyury expression compared to Wnt activation with Wnt3a and CHIR-99021 (Figure 5G), which is consistent with previous studies (Bernardo et al., 2011; Turner et al., 2017). However, BMP4 and Activin A treatment failed to induce Brachyury expression in *Dvl* TKO EBs (Figure 5D, 5E, 5G), suggesting that Wnt activation is required to initiate differentiation while BMP and Nodal signaling act synergistically with Wnt to promote mesoderm expansion.

Overall, we found that without Wnt activity mediated by the Dvls, BMP and Nodal signaling activation are unable to rescue the defects in mesoderm differentiation in the *Dvl* TKO EBs. In *WT* EBs, Wnt and BMP signaling appear to initiate mesoderm differentiation, as stimulation by CHIR-99021 and BMP4, respectively, led to earlier Brachyury expression compared to the untreated controls. Nodal activation did not affect the time of mesoderm induction, but rather appears to act synergistically to enhance expansion of the mesodermal cell population.

Inhibition of Canonical Wnt, BMP, and Nodal Signaling in *WT* Embryoid Bodies Phenocopies Mesoderm Differentiation Defects in *Dvl* TKO EBs

To determine if the mesoderm defects in the *Dvl* TKO EBs can be recapitulated in *WT* EBs, we inhibited the Wnt, BMP, and Nodal signaling pathways in *WT* EBs during the first 2 days of EB formation (Figure 6, Supplemental Figure 2A–C). Interestingly, when compared to the untreated control, the overall areas of *WT* EBs treated with BMP (LDN-193189) and canonical/non-canonical Wnt (IWP L6) inhibitors did not increase over time, whereas Nodal inhibition (SB-431542) did not significantly impact EB size (Supplemental Figure 2B, 2D). Compared to the untreated control, *Dvl* TKO EBs appeared to be unaffected by these inhibitors, and remained smaller than *WT* EBs (Supplemental Figure 2C, 2D). Importantly, we were unable to detect Brachyury-positive cells by IHC in *WT* EBs treated with LDN-193189, IWP L6, and SB-431542 throughout the differentiation time course, even after the drugs were removed on day 2 (Figure 6A, 6C). Furthermore, suppression of BMP and canonical/non-canonical Wnt pathways led to an attenuation of Brachyury expression (Figure 6E). However, Nodal signaling inhibition with SB-431542 did not completely diminish Brachyury levels in the *WT* EBs (Figure 6E). As expected, treatment of *Dvl* TKO EBs with these inhibitors did not affect Brachyury expression over time (Figure 6B–C). Altogether, these results further support that mesoderm induction is driven by Wnt and BMP signaling, while Nodal signaling acts synergistically to reinforce mesodermal fate specification rather than directly regulate mesoderm induction.

Decreased Wnt and BMP Signaling in the Absence of the *Dvls* Enhances Endoderm Differentiation

The *in vivo* effects of complete *Dvl* loss on endoderm differentiation was previously unknown due to early embryonic lethality. Therefore, we measured the mRNA levels of GATA4 over the time course of EB formation to determine the differences in endoderm differentiation potential. Spontaneous endoderm differentiation was low in untreated *WT* and *Dvl* TKO EBs with GATA4 expression near baseline throughout the differentiation time course (Figure 5H). BMP4 stimulation overall did not result in significant increases in GATA4, except in *Dvl* TKO EBs on day 2 (Figure 5H). Since the EBs were treated with each drug for 48 h, the spike in GATA4 in the *Dvl* TKO EBs may be an effect of direct BMP4 stimulation to induce earlier endoderm differentiation. However, beyond day 2, the GATA4 levels remain near baseline (Figure 5H), suggesting that the transient increase may be an artifact of culture, rather than an indication of early endoderm differentiation.

Wnt activation during differentiation led to increases in GATA4 in *WT* and *Dvl* TKO EBs, with CHIR-99021 treatment resulting in higher expression levels than Wnt3a (Figure 5H). We anticipated that the *Dvl* TKO EBs treated with CHIR-99021 would result in similar GATA4 expression levels as *WT* EBs. However, CHIR-treated *Dvl* TKO EBs displayed a 20-fold increase in GATA4 compared to the untreated controls and approximately 2 to 5-fold higher GATA4 compared to CHIR-treated *WT* EBs throughout the differentiation time course (Figure 5H). Surprisingly, Wnt3a appeared to increase GATA4 expression over time in *Dvl* TKO EBs, which may indicate that Wnt3a can function independently of Dvl-mediated Wnt activation to induce endoderm differentiation.

Nodal signaling activation by Activin A promotes endoderm differentiation *in vitro* (D'Amour et al., 2005; Kraus and Grapin-Botton, 2012; Loh et al., 2014). By day 6 of differentiation, the expression of GATA6 was increased in Activin A-treated *WT* and *Dvl* TKO EBs by 3-fold and 6-fold, respectively, compared to the untreated controls (Figure 5H).

It is likely that the signaling dynamics that promote robust mesoderm activation in the EBs may have antagonistic effects on endoderm differentiation in culture (Bernardo et al., 2011; Loebel et al., 2003; Loh et al., 2014). Since BMP4 and Activin A treatment enhanced mesoderm differentiation in *WT* EBs (Figures 5G), we tested whether inhibition BMP and Nodal signaling could induce endoderm differentiation. Indeed, we found that LDN-193189 and SB-431542 treatments, which inhibited mesoderm differentiation (Figure 6E), resulted in increased GATA4 expression in *WT* EBs (Figure 6F). BMP inhibition, in particular, promoted earlier and enhanced endoderm differentiation (Figure 6F). The *Dvl* TKO EBs treated with LDN-193189 displayed even greater GATA4 mRNA levels compared to *WT* (Figure 6F), which prompted us to test whether inhibition of Wnt also promoted endoderm differentiation. While the increased GATA4 expression in the presence of Wnt3a and CHIR-99021 suggests that activation of Wnt is required for endoderm formation, we found that IWP L6 treatment led to even more robust GATA4 expression (Figure 6F). Notably, IWP L6-treated *Dvl* TKO EBs displayed a 41 to 188-fold increase in GATA4 during the differentiation process and was much more pronounced than IWP L6-treated *WT* EBs (Figure 6F). While Wnt signaling is involved in endoderm development, these results suggest that antagonizing mesoderm induction by inhibiting BMP and Wnt signaling promotes endoderm differentiation and supports previous published findings (Loebel et al., 2003; Loh et al., 2014; Vallier et al., 2009).

Absence of the *Dvls* Does Not Prevent Ectoderm Differentiation

During spontaneous differentiation, pluripotent cells adopt an ectodermal and neural fate by default (Lenka and Ramasamy, 2007; Munoz-Sanjuan and Brivanlou, 2002). Suppression of canonical Wnt, BMP, and Nodal signaling promotes ectoderm differentiation while inhibiting mesoderm formation (Arkell et al., 2013; Li et al., 2013; Liu et al., 2018; Patani et al., 2009; Patthey and Gunhaga, 2014; Vallier et al., 2004). Therefore, we expected to observe enhanced ectodermal differentiation and increased expression of the ectoderm marker, Otx2, in the *Dvl* TKO EBs, which also have decreased BMP signaling (Figure 5A). However, there were no significant differences in Otx2-positive cells at the protein level in the *Dvl* TKO EBs with or without drug treatment (Figure 5F, 6D).

We mainly observed a delay in the down-regulation of Otx2 mRNA in *Dvl* TKO EBs, rather than enhanced expression (Supplemental Figure 3). In the untreated EBs, Otx2 expression was maintained in the *Dvl* TKO EBs from days 2–5, while in *WT* EBs, Otx2 declined throughout the differentiation process (Figure 4I). Activation of canonical Wnt, BMP, and Nodal signaling further decreased Otx2 expression in *WT* EBs compared to the untreated controls, but BMP4, Wnt3a, and Activin A treatments led to a delay in Otx2 suppression in *Dvl* TKO EBs (Supplemental Figure 3). Wnt3a, which does not activate canonical Wnt signaling in the *Dvl* TKO EBs, did not suppress Otx2 levels, whereas CHIR-99021 treatment resulted in similar Otx2 expression in *Dvl* TKO as *WT* EBs (Supplemental Figure 3). It is

possible that BMP4 and Activin A treatment may lead to secondary effects that delay ectoderm suppression in the absence of the *Dvls* and mesoderm differentiation.

Inhibition of BMP (LDN-193189) and Wnt (IWP L6) and Nodal (SB-431542) all led to a delay in the decline of Otx2 expression in *WT* and *Dvl* TKO EBs, but did not enhance Otx2 expression over the course of differentiation (Supplemental Figure 3). The *WT* EBs morphologically resembled the *Dvl* TKO EBs by forming the outer ectodermal ring of cells (Supplemental Figure 2B) and displayed reduced proliferation over time (Supplemental Figure 2D). Although the differences in Otx2 expression in *WT* and *Dvl* TKO EBs were minor, these results demonstrate that the absence of the *Dvls* does not inhibit ectoderm differentiation.

Discussion

The *Dishevelleds* Are Required During Early Embryonic Development

Complete disruption of the *Dvl* genes has profound consequences on early embryonic development since they are required to transduce canonical and non-canonical Wnt signaling. Despite their functional redundancy, we found that the severity of A-P axis specification and mesoderm formation defects increases as the dosage of the *Dvl* genes decreases. Using a 3D embryoid body system allowed us to model germ lineage differentiation *in vitro* and identify a plethora of dysregulated genes that impact A-P pattern specification, gastrulation induction, mesoderm formation and its derived tissues. Furthermore, we demonstrate that activating canonical Wnt, BMP, and Nodal signaling in the absence of the *Dvls* fails to rescue mesodermal differentiation, suggesting a potential role of Wnt/PCP signaling in regulating mesoderm development.

Other studies have sought to disrupt both canonical and non-canonical signaling to determine the effects on early development though deletion of *Porcupine* (*Porcn*), which is a non-redundant gene required for Wnt ligand secretion (Barrott et al., 2011; Biechele et al., 2013; Biechele et al., 2011). However, the observed phenotypes of the $Porcn^{-/-}$ mutants are less severe than the *Dvl* TKO, $\beta\text{-}catenin^{-/-}$ and $mpk1^{-/-}$ mutants, in which both axis specification and mesoderm induction are defective. Rather, $Porcn^{-/-}$ resemble $Wnt3^{-/-}$ mutants that undergo proper A-P specification but lack mesoderm differentiation (Biechele et al., 2013; Biechele et al., 2011). Reduced canonical Wnt reporter activity was confirmed in these embryos, but the impact on non-canonical Wnt is unknown. A recent study demonstrated that Porcn activity might not be required for all Wnt ligand secretion, suggesting that its function may be context-dependent (Richards et al., 2014). As such, it is possible that *Porcn* deletion might not simultaneously disrupt both Wnt signaling pathways, which would explain the development of their less severe phenotypes compared to the *Dvl* TKO embryos.

In another study by Soares et al. (2005), Dvl1, Dvl2, and Dvl3 were knocked down using RNAi during pre-implantation. The Dvl knock-down embryos displayed developmental delay, but gastrulation induction and mesodermal differentiation remained intact in 60% of analyzed embryos. These embryos retained approximately 24–30% expression of each Dvl, which may have been sufficient to maintain Wnt signaling in a redundant manner (Soares et

al., 2005). Dvl knock-down embryos displayed normal Brachyury expression in contrast to our observations in *Dvl2*$^{-/-}$*; Dvl3*$^{-/-}$, *Dvl1*$^{+/-}$*; Dvl2*$^{-/-}$*; Dvl3*$^{-/-}$ and *Dvl* TKO embryos.

It is unclear why the *Dvl1*$^{+/-}$*; Dvl2*$^{-/-}$*; Dvl3*$^{-/-}$ embryos exhibit varying severities of defective axis specification where a subset of embryos had undergone proper A-P formation. We have previously observed variable or incompletely penetrant phenotypes in single and double *Dvl* mutants, such as the 50% penetrant conotruncal defects displayed by *Dvl2*$^{-/-}$ embryos (Hamblet et al., 2002). It is possible that differing levels of maternal Dvl exposure could potentially compensate for some of the developmental defects, or that non-genetic effects are responsible for the variable expressivity in *Dvl* mutants. Despite the heterogeneous defects observed in the *Dvl1*$^{+/-}$*; Dvl2*$^{-/-}$*; Dvl3*$^{-/-}$ embryos, it is clear that a single allele of *Dvl* is sufficient to induce mesoderm differentiation, but fails to organize proper mesoderm patterning. Furthermore, the lack of Brachyury and Lefty1 expression in the *Dvl* TKO embryos reinforce the importance of the *Dvls* in regulating DVE migration for axis specification and patterning during gastrulation.

The *Dishevelleds* Are Not Required for Maintaining Self-Renewal in mESCs

Several studies have proposed that canonical Wnt signaling is an important regulator of self-renewal in mouse ESCs (Hao et al., 2006; Ogawa et al., 2006; Sato et al., 2004), as activation of canonical Wnt signaling by GSK3 inhibition can increase the efficiency of somatic cell reprogramming (Wray et al., 2011) and β-catenin can regulate the activities of Oct4 and Nanog to reinforce pluripotency (Faunes et al., 2013; Kelly et al., 2011). However, other studies have shown that the transcriptional activity of canonical Wnt is repressed during pre-implantation development and is not required for the expression of pluripotency markers in human and mouse ESCs (Davidson et al., 2012; Lyashenko et al., 2011; Na et al., 2007; Xu et al., 2016). Furthermore, Wnt mutants, such as *β-catenin*$^{-/-}$ embryos, are also capable of survival past pre-implantation, and *β-catenin*$^{-/-}$ mESCs are viable and retain self-renewal properties (Haegel et al., 1995; Huelsken et al., 2000; Lyashenko et al., 2011). Overall, these conflicting studies highlight the dynamic nature of Wnt signaling during development that is both context-and time-dependent.

Our studies that eliminate Dvl-dependent Wnt signaling further support the notion that Wnt signaling is not required to maintain a state of self-renewal in mESCs. *Dvl* TKO mESCs express pluripotent markers and continue to exhibit self-renewal properties for over 20 passages without spontaneously differentiating. In addition, *Dvl* TKO embryos survive through the pre-implantation, further suggesting that Dvl-mediated Wnt activity is dispensable at this stage of development.

Loss of the *Dishevelleds* Selectively Disrupts Mesoderm Induction but is Permissive for Endoderm and Ectoderm Differentiation

Due to the early lethality in the *Dvl* TKO embryos, we took advantage of using an EB system where we were able to recapitulate the mesodermal defects and demonstrate that endoderm and ectoderm differentiation is induced in the absence of Dvl-mediated Wnt signaling. We expected ectoderm differentiation to remain intact since *β-catenin*$^{-/-}$ embryos and EBs are able to form ectodermal tissues (Haegel et al., 1995; Huelsken et al., 2000;

Lyashenko et al., 2011). However, it was surprising that *Dvl* TKO EBs were able to undergo endoderm differentiation, given that Wnt signaling is involved in its development. In addition, Wnt3a treatment, which would not activate Wnt signaling in the *Dvl* TKO EBs, resulted in increased GATA4 expression. It is possible that Wnt3a may exert its effects independently of the Dvls. Furthermore, endoderm differentiation potential was further enhanced with BMP inhibition. Although the *Dvls* appear to be dispensable for endoderm differentiation, it is likely that *in vivo* these germ lineages will harbor defects in endoderm patterning and morphogenesis without sustained Wnt signaling. Mutants with conditional *β-catenin* deletion in Sox17 lineage cells were able to specify definitive endoderm identity, but ultimately failed to properly form the endoderm germ layer (Engert et al., 2013). Additional studies would be needed to further confirm *in vivo* endodermal defects in *Dvl* TKO embryos.

Intersection of Dvl-Mediated Wnt Signaling with BMP and Nodal Developmental Pathways During Lineage Differentiation

We demonstrate that the Dvls are necessary to regulate BMP and Wnt signaling to induce mesoderm, and loss of this signaling activity helps to drive endoderm differentiation (Figure 7A). Activation of BMP, canonical Wnt, and Nodal signaling was insufficient to rescue the mesodermal differentiation defects in *Dvl* TKO EBs, but inhibition of these pathways in *WT* EBs phenocopied the lineage differentiation potentials of *Dvl* TKO EBs (Figure 7B–C). Moreover, the down-regulation of key BMP signaling genes and dysregulation of Nodal-associated genes in the *Dvl* TKO EBs (Figure 5, Figure 7A) could also contribute to a refractory response to BMP4 and Activin A treatment, which would further prevent phenotypic rescue.

In the *Dvl* TKO EBs, the reduced capacity of BMP and Wnt signaling, which in turn feed back to Nodal pathway activation, led to suppression of mesoderm differentiation, but it had the opposite effect on endoderm and ectoderm differentiation (Figure 7B). *Dvl* TKO EBs displayed increased endoderm differentiation potential compared to *WT* EBs. Furthermore, the decreased BMP response in *Dvl* TKO EBs may have enhanced the effects of the BMP inhibitor, LDN-193189, as well as worked synergistically with the Wnt inhibitor, IWP L6, to promote endoderm differentiation (Figure 7A–B).

Despite the lack of significant differences in ectoderm differentiation in *WT* and *Dvl* TKO EBs, we observed a delay in the decreased ectodermal lineage potential in *Dvl* TKO EBs (Figure 7B). Even in the presence of BMP4 and Activin A stimulation, which typically inhibit ectodermal fate, *Dvl* TKO EBs displayed slightly increased ectoderm differentiation potential compared to *WT* EBs. It is possible that these drugs might have secondary effects that lead to the transient increase in ectoderm potential. We observed similar trends in gene expression between *Dvl* TKO and *WT* EBs treated with the inhibitors, suggesting that modulating these pathways does have a biological effect on ectoderm differentiation (Figure 7B–C). Alternative 3D culture systems, such as cerebral organoids, may be more suitable to determine the differences in ectoderm differentiation.

Potential Role for Wnt/PCP Signaling

We have previously shown that PCP-specific phenotypes occur in the single, double, and triple *Dvl1/2/3* mutants. With the exception of the abnormal behavioral phenotypes, which appear to be the result of canonical Wnt signaling (Belinson et al., 2016), we demonstrate that a number of the developmental defects in the brain, neural tube, somites, heart, and inner ear are caused by PCP effects (Etheridge et al., 2008; Hamblet et al., 2002; Ohata et al., 2014; Wang et al., 2006). Based on these studies, we have strong evidence to expect that the complete triple *Dvl* KO embryos display PCP-associated defects.

When we systematically tested whether activating BMP, Nodal, or canonical Wnt signaling in the *Dvl* TKO EBs could rescue mesoderm differentiation, we found that none of the small molecule activators, particularly CHIR99021, could maintain Brachyury expression. In addition, the suppression of Brachyury expression in *WT* EBs with IWP treatment is likely to be a consequence of disrupting both Wnt signaling pathways, not solely due to canonical Wnt signaling inhibition. Previous studies have demonstrated that deletion of JNK1/2 in mESCs result in mesoderm differentiation defects in teratoma formation assays (Xu and Davis, 2010). Furthermore, the treatment of pre-gastrulating rabbit embryos with the Rock inhibitor, Y-27632, results in deformation of the primitive streak and inhibits Brachyury expression in a dose-dependent manner (Stankova et al., 2015). Altogether, these studies provide evidence that the activation of PCP downstream of the Dvls is involved in mesoderm differentiation and Brachyury expression, in addition to canonical Wnt signaling.

Whether Wnt/PCP activates or represses canonical Wnt signaling activity may be context-dependent. Previous studies suggest that activation of Wnt/PCP by Wnt5a binding to Ror2 may repress canonical Wnt signaling by regulating β-catenin stability and expression (Mikels and Nusse, 2006; Topol et al., 2003) or through competition for Dvl binding (van Amerongen and Nusse, 2009). Conversely, other work has shown that activation by Wnt8a binding to Ror2 can control paracrine Wnt/β-catenin activation through the formation of cytonemes (Mattes et al., 2018). Moreover, the AVE and mesodermal defects that arise in Wnt/PCP mutants, such as $mpk1^{-/-}$ (Tao et al., 2009) and $Rac1^{-/-}$ (Migeotte et al., 2011; Migeotte et al., 2010), closely resemble the phenotypes observed in $\beta\text{-}catenin^{-/-}$ mutants as well as the *Dvl* TKO mutants. The similarity in phenotypes that manifest when these two independent pathways are perturbed would suggest that the Wnt pathways must interact on some level to regulate development. Additional studies are needed to better understand the differential roles and crosstalk between the Wnt pathways.

In our studies, we found that the gene expression of *Ror2*, *Wnt5a*, *Wnt8a*, and other core PCP components were all significantly down-regulated in the *Dvl* TKO EBs (Figure 3E). If Wnt/PCP signaling through Ror2 and the Dvls does indeed play a role in regulating canonical Wnt activation during mesoderm development, it would partially explain why CHIR99021 treatment alone was not sufficient to rescue the *Dvl* TKO defects. Alternatively, perhaps a certain threshold of Wnt/β-catenin and/or Wnt/PCP signaling is required to induce and maintain mesoderm formation, based on the increasing severity of developmental phenotypes that arise as the gene dosage of *Dvl* decreases.

Signaling Crosstalk of Developmental Pathways

While the crosstalk between canonical Wnt, BMP, and Nodal have been extensively studied in a number of different developmental contexts (reviewed in (Itasaki and Hoppler, 2010; Luo, 2017)), the role of Wnt/PCP in the regulation of BMP and Nodal signaling activity is unclear. There was decreased expression of key BMP signaling genes in the *Dvl* TKO EBs, but we could not definitively determine if this was due to the disruption of canonical and/or non-canonical Wnt signaling. The interaction of Wnt/PCP and BMP signaling has been implicated in limb development (Bernatik et al., 2017; Wang et al., 2012) where mutations in *Ror2* and *Noggin* lead to similar brachydactyly disorders.

In addition, Nodal signaling has been implicated in regulating the expression of Dvl2 to the lateral plasma membrane of epiblast visceral endodermal cells to activate PCP signaling (Trichas et al., 2011). Disrupting Dvl2 planar polarization resulted in abnormal AVE migration onto the extra-embryonic ectoderm (Trichas et al., 2011). Furthermore, *Nodal* null mutants displayed reduced membrane localization of Dvl2, while *Lefty1* null mutants resulted in increased ectopic Dvl2 localization (Trichas et al., 2011). The role of PCP signaling during early development has been underappreciated and challenging to study since no direct gene targets have been identified to date. Our studies suggest that PCP signaling may also be crucial for axis specification, germ lineage differentiation, and patterning. Additional work is needed to better understand how PCP signaling is integrated into the overall developmental signaling network to regulate early developmental processes.

Conclusion

These studies highlight the importance of the *Dvl* genes in regulating early developmental processes. Loss of the *Dvls* does not negatively impact pre-implantation development or self-renewal properties in mESCs. However, proper gene dosage of the *Dvls* is required to establish a certain threshold of Wnt signaling to regulate A-P axis specification, gastrulation induction, and mesoderm differentiation. Deletion of the *Dvls* leads to down-regulation of key BMP signaling genes, which specifically exacerbates the defects in mesoderm induction, while endoderm and ectoderm differentiation remain intact. Our results suggest that Wnt/PCP signaling may also play a major role during gastrulation since activation of BMP, Nodal, and canonical Wnt signaling failed to rescue the mesodermal defects in *Dvl* TKO EBs.

Supplementary Material

Refer to Web version on PubMed Central for supplementary material.

Acknowledgements

Richard Lee in the CWRU SOM Light Microscopy Core Facility funded by NIH Grant S10-RR021228 assisted in the imaging studies, and George Lee provided crucial assistance in high-throughput image segmentation and image analysis of the EBs and immunofluorescence staining. We thank Radika Atit, Peter Scacheri, and Paul Tesar for their insights and comments on the manuscript. This work was funded in part by NIH grant R01MH114601.

References

Andre P, Song H, Kim W, Kispert A, Yang Y, 2015. Wnt5a and Wnt11 regulate mammalian anterior-posterior axis elongation. Development 142, 1516–1527. [PubMed: 25813538]

Arkell RM, Fossat N, Tam PP, 2013. Wnt signalling in mouse gastrulation and anterior development: new players in the pathway and signal output. Curr Opin Genet Dev 23, 454–460. [PubMed: 23608663]

Arnold SJ, Robertson EJ, 2009. Making a commitment: cell lineage allocation and axis patterning in the early mouse embryo. Nature Reviews Molecular Cell Biology 10, 91–103. [PubMed: 19129791]

Ashburner M, Ball CA, Blake JA, Botstein D, Butler H, Cherry JM, Davis AP, Dolinski K, Dwight SS, Eppig JT, Harris MA, Hill DP, Issel-Tarver L, Kasarskis A, Lewis S, Matese JC, Richardson JE, Ringwald M, Rubin GM, Sherlock G, 2000. Gene Ontology: tool for the unification of biology. Nature Genetics 25, 25–29. [PubMed: 10802651]

Barrott JJ, Cash GM, Smith AP, Barrow JR, Murtaugh LC, 2011. Deletion of mouse Porcn blocks Wnt ligand secretion and reveals an ectodermal etiology of human focal dermal hypoplasia/Goltz syndrome. Proceedings of the National Academy of Sciences 108, 12752–12757.

Barrow JR, Howell WD, Rule M, Hayashi S, Thomas KR, Capecchi MR, McMahon AP, 2007. Wnt3 signaling in the epiblast is required for proper orientation of the anteroposterior axis. Developmental Biology 312, 312–320. [PubMed: 18028899]

Belinson H, Nakatani J, Babineau BA, Birnbaum RY, Ellegood J, Bershteyn M, McEvilly RJ, Long JM, Willert K, Klein OD, Ahituv N, Lerch JP, Rosenfeld MG, Wynshaw-Boris A, 2016. Prenatal beta-catenin/Brn2/Tbr2 transcriptional cascade regulates adult social and stereotypic behaviors. Mol Psychiatry 21, 1417–1433. [PubMed: 26830142]

Bernardo AS, Faial T, Gardner L, Niakan KK, Ortmann D, Senner CE, Callery EM, Trotter MW, Hemberger M, Smith JC, Bardwell L, Moffett A, Pedersen RA, 2011. BRACHYURY and CDX2 mediate BMP-induced differentiation of human and mouse pluripotent stem cells into embryonic and extraembryonic lineages. Cell Stem Cell 9, 144–155. [PubMed: 21816365]

Bernatik O, Radaszkiewicz T, Behal M, Dave Z, Witte F, Mahl A, Cernohorsky NH, Krejci P, Stricker S, Bryja V, 2017. A Novel Role for the BMP Antagonist Noggin in Sensitizing Cells to Non-canonical Wnt-5a/Ror2/Disheveled Pathway Activation. Front Cell Dev Biol 5, 47. [PubMed: 28523267]

Biechele S, Cockburn K, Lanner F, Cox BJ, Rossant J, 2013. Porcn-dependent Wnt signaling is not required prior to mouse gastrulation. Development 140, 2961–2971. [PubMed: 23760955]

Biechele S, Cox BJ, Rossant J, 2011. Porcupine homolog is required for canonical Wnt signaling and gastrulation in mouse embryos. Developmental Biology 355, 275–285. [PubMed: 21554866]

Boutros M, Mlodzik M, 1999. Dishevelled: at the crossroads of divergent intracellular signaling pathways. Mech Dev 83, 27–37. [PubMed: 10507837]

Bryja V, Bonilla S, Arenas E, 2006. Derivation of mouse embryonic stem cells. Nature Protocols 1, 2082–2087. [PubMed: 17487198]

Clevers H, Nusse R, 2012. Wnt/beta-catenin signaling and disease. Cell 149, 1192–1205. [PubMed: 22682243]

Coucouvanis E, Martin GR, 1999. BMP signaling plays a role in visceral endoderm differentiation and cavitation in the early mouse embryo. Development 126, 535–546. [PubMed: 9876182]

D'Amour KA, Agulnick AD, Eliazer S, Kelly OG, Kroon E, Baetge EE, 2005. Efficient differentiation of human embryonic stem cells to definitive endoderm. Nat Biotechnol 23, 1534–1541. [PubMed: 16258519]

Davidson KC, Adams AM, Goodson JM, McDonald CE, Potter JC, Berndt JD, Biechele TL, Taylor RJ, Moon RT, 2012. Wnt/ -catenin signaling promotes differentiation, not self-renewal, of human embryonic stem cells and is repressed by Oct4. Proceedings of the National Academy of Sciences 109, 4485–4490.

Engert S, Burtscher I, Liao WP, Dulev S, Schotta G, Lickert H, 2013. Wnt/beta-catenin signalling regulates Sox17 expression and is essential for organizer and endoderm formation in the mouse. Development 140, 3128–3138. [PubMed: 23824574]

Etheridge SL, Ray S, Li S, Hamblet NS, Lijam N, Tsang M, Greer J, Kardos N, Wang J, Sussman DJ, Chen P, Wynshaw-Boris A, 2008. Murine dishevelled 3 functions in redundant pathways with dishevelled 1 and 2 in normal cardiac outflow tract, cochlea, and neural tube development. PLoS Genet 4, e1000259. [PubMed: 19008950]

Faunes F, Hayward P, Descalzo SM, Chatterjee SS, Balayo T, Trott J, Christoforou A, Ferrer-Vaquer A, Hadjantonakis AK, Dasgupta R, Arias AM, 2013. A membrane-associated -catenin/Oct4 complex correlates with ground-state pluripotency in mouse embryonic stem cells. Development 140, 1171–1183. [PubMed: 23444350]

Fiedler M, Mendoza-Topaz C, Rutherford TJ, Mieszczanek J, Bienz M, 2011. Dishevelled interacts with the DIX domain polymerization interface of Axin to interfere with its function in down-regulating beta-catenin. Proc Natl Acad Sci U S A 108, 1937–1942. [PubMed: 21245303]

Gaztelumendi N, Nogues C, 2014. Chromosome instability in mouse embryonic stem cells. Sci Rep 4, 5324. [PubMed: 24937170]

Haegel H, Larue L, Ohsugi M, Fedorov L, Herrenknecht K, Kemler R, 1995. Lack of beta-catenin affects mouse development at gastrulation. Development 121, 3529–3537. [PubMed: 8582267]

Hamblet NS, Lijam N, Ruiz-Lozano P, Wang J, Yang Y, Luo Z, Mei L, Chien KR, Sussman DJ, Wynshaw-Boris A, 2002. Dishevelled 2 is essential for cardiac outflow tract development, somite segmentation and neural tube closure. Development 129, 5827–5838. [PubMed: 12421720]

Hao J, Li TG, Qi X, Zhao DF, Zhao GQ, 2006. WNT/beta-catenin pathway up-regulates Stat3 and converges on LIF to prevent differentiation of mouse embryonic stem cells. Dev Biol 290, 81–91. [PubMed: 16330017]

Hashimoto M, Shinohara K, Wang J, Ikeuchi S, Yoshiba S, Meno C, Nonaka S, Takada S, Hatta K, Wynshaw-Boris A, Hamada H, 2010. Planar polarization of node cells determines the rotational axis of node cilia. Nat Cell Biol 12, 170–176. [PubMed: 20098415]

Ho HYH, Susman MW, Bikoff JB, Ryu YK, Jonas AM, Hu L, Kuruvilla R, Greenberg ME, 2012. Wnt5a-Ror-Dishevelled signaling constitutes a core developmental pathway that controls tissue morphogenesis. Proceedings of the National Academy of Sciences 109, 4044–4051.

Huelsken J, Vogel R, Brinkmann V, Erdmann B, Birchmeier C, Birchmeier W, 2000. Requirement for β-Catenin in Anterior-Posterior Axis Formation in Mice. The Journal of Cell Biology 148, 567–578. [PubMed: 10662781]

Itasaki N, Hoppler S, 2010. Crosstalk between Wnt and bone morphogenic protein signaling: a turbulent relationship. Dev Dyn 239, 16–33. [PubMed: 19544585]

Kelly KF, Ng DY, Jayakumaran G, Wood GA, Koide H, Doble BW, 2011. β-Catenin Enhances Oct-4 Activity and Reinforces Pluripotency through a TCF-Independent Mechanism. Cell Stem Cell 8, 214–227. [PubMed: 21295277]

Kelly OG, P. KI, S. WC, 2004. The Wnt co-receptors Lrp5 and Lrp6 are essential for gastrulation in mice. Development 131, 2803–2815. [PubMed: 15142971]

Kim D, Langmead B, Salzberg SL, 2015. HISAT: a fast spliced aligner with low memory requirements. Nature Methods 12, 357–360. [PubMed: 25751142]

Kimelman D, Xu W, 2006. beta-catenin destruction complex: insights and questions from a structural perspective. Oncogene 25, 7482–7491. [PubMed: 17143292]

Kishida S, Yamamoto H, Hino S, Ikeda S, Kishida M, Kikuchi A, 1999. DIX domains of Dvl and axin are necessary for protein interactions and their ability to regulate beta-catenin stability. Mol Cell Biol 19, 4414–4422. [PubMed: 10330181]

Kispert A, Herrmann BG, 1994. Immunohistochemical Analysis of the Brachyury Protein in Wild-Type and Mutant Mouse Embryos. Developmental Biology 161, 179–193. [PubMed: 8293872]

Kraus MR, Grapin-Botton A, 2012. Patterning and shaping the endoderm in vivo and in culture. Curr Opin Genet Dev 22, 347–353. [PubMed: 22742850]

Kurokawa D, Takasaki N, Kiyonari H, Nakayama R, Kimura-Yoshida C, Matsuo I, Aizawa S, 2004. Regulation of Otx2 expression and its functions in mouse epiblast and anterior neuroectoderm. Development 131, 3307–3317. [PubMed: 15201223]

Lenka N, Ramasamy SK, 2007. Neural induction from ES cells portrays default commitment but instructive maturation. PLoS One 2, e1349. [PubMed: 18092007]

Li H, Handsaker B, Wysoker A, Fennell T, Ruan J, Homer N, Marth G, Abecasis G, Durbin R, 2009. The Sequence Alignment/Map format and SAMtools. Bioinformatics 25, 2078–2079. [PubMed: 19505943]

Li L, Liu C, Biechele S, Zhu Q, Song L, Lanner F, Jing N, Rossant J, 2013. Location of transient ectodermal progenitor potential in mouse development. Development 140, 4533–4543. [PubMed: 24131634]

Lijam N, Paylor R, McDonald MP, Crawley JN, Deng CX, Herrup K, Stevens KE, Maccaferri G, McBain CJ, Sussman DJ, Wynshaw-Boris A, 1997. Social interaction and sensorimotor gating abnormalities in mice lacking Dvl1. Cell 90, 895–905. [PubMed: 9298901]

Liu C, Wang R, He Z, Osteil P, Wilkie E, Yang X, Chen J, Cui G, Guo W, Chen Y, Peng G, Tam PPL, Jing N, 2018. Suppressing Nodal Signaling Activity Predisposes Ectodermal Differentiation of Epiblast Stem Cells. Stem Cell Reports 11, 43–57. [PubMed: 30008328]

Liu P, Wakamiya M, Shea MJ, Albrecht U, Behringer RR, Bradley A, 1999. Requirement for Wnt3 in vertebrate axis formation. Nature Genetics 22, 361–365. [PubMed: 10431240]

Loebel DA, Watson CM, De Young RA, Tam PP, 2003. Lineage choice and differentiation in mouse embryos and embryonic stem cells. Dev Biol 264, 1–14. [PubMed: 14623228]

Loh KM, Ang LT, Zhang J, Kumar V, Ang J, Auyeong JQ, Lee KL, Choo SH, Lim CY, Nichane M, Tan J, Noghabi MS, Azzola L, Ng ES, Durruthy-Durruthy J, Sebastiano V, Poellinger L, Elefanty AG, Stanley EG, Chen Q, Prabhakar S, Weissman IL, Lim B, 2014. Efficient endoderm induction from human pluripotent stem cells by logically directing signals controlling lineage bifurcations. Cell Stem Cell 14, 237–252. [PubMed: 24412311]

Love MI, Huber W, Anders S, 2014. Moderated estimation of fold change and dispersion for RNA-seq data with DESeq2. Genome Biology 15.

Luo K, 2017. Signaling Cross Talk between TGF-beta/Smad and Other Signaling Pathways. Cold Spring Harb Perspect Biol 9.

Lyashenko N, Winter M, Migliorini D, Biechele T, Moon RT, Hartmann C, 2011. Differential requirement for the dual functions of β-catenin in embryonic stem cell self-renewal and germ layer formation. Nature Cell Biology 13, 753–761. [PubMed: 21685890]

Martin M, 2011. Cutadapt removes adapter sequences from high-throughput sequencing reads. EMBnet.journal 17, 10.

Mattes B, Dang Y, Greicius G, Kaufmann LT, Prunsche B, Rosenbauer J, Stegmaier J, Mikut R, Özbek S, Nienhaus GU, Schug A, Virshup DM, Scholpp S, 2018. Wnt/PCP controls spreading of Wnt/β-catenin signals by cytonemes in vertebrates. eLife 7.

Migeotte I, Grego-Bessa J, Anderson KV, 2011. Rac1 mediates morphogenetic responses to intercellular signals in the gastrulating mouse embryo. Development 138, 3011–3020. [PubMed: 21693517]

Migeotte I, Omelchenko T, Hall A, Anderson KV, 2010. Rac1-dependent collective cell migration is required for specification of the anterior-posterior body axis of the mouse. PLoS Biol 8, e1000442. [PubMed: 20689803]

Mikels AJ, Nusse R, 2006. Purified Wnt5a Protein Activates or Inhibits β-Catenin–TCF Signaling Depending on Receptor Context. PLoS Biology 4, e115. [PubMed: 16602827]

Morkel M, 2003. -Catenin regulates Cripto- and Wnt3-dependent gene expression programs in mouse axis and mesoderm formation. Development 130, 6283–6294. [PubMed: 14623818]

Munoz-Sanjuan I, Brivanlou AH, 2002. Neural induction, the default model and embryonic stem cells. Nat Rev Neurosci 3, 271–280. [PubMed: 11967557]

Na J, Lykke-Andersen K, Torres Padilla ME, Zernicka-Goetz M, 2007. Dishevelled proteins regulate cell adhesion in mouse blastocyst and serve to monitor changes in Wnt signaling. Developmental Biology 302, 40–49. [PubMed: 17005174]

Nusse R, Clevers H, 2017. Wnt/beta-Catenin Signaling, Disease, and Emerging Therapeutic Modalities. Cell 169, 985–999. [PubMed: 28575679]

Ogawa K, Nishinakamura R, Iwamatsu Y, Shimosato D, Niwa H, 2006. Synergistic action of Wnt and LIF in maintaining pluripotency of mouse ES cells. Biochem Biophys Res Commun 343, 159–166. [PubMed: 16530170]

Ohata S, Nakatani J, Herranz-Pérez V, Cheng J, Belinson H, Inubushi T, Snider William D., García-Verdugo Jose M., Wynshaw-Boris A, Álvarez-Buylla A, 2014. Loss of Dishevelleds Disrupts Planar Polarity in Ependymal Motile Cilia and Results in Hydrocephalus. Neuron 83, 558–571. [PubMed: 25043421]

Patani R, Compston A, Puddifoot CA, Wyllie DJ, Hardingham GE, Allen ND, Chandran S, 2009. Activin/Nodal inhibition alone accelerates highly efficient neural conversion from human embryonic stem cells and imposes a caudal positional identity. PLoS One 4, e7327. [PubMed: 19806200]

Patthey C, Gunhaga L, 2014. Signaling pathways regulating ectodermal cell fate choices. Exp Cell Res 321, 11–16. [PubMed: 23939346]

Pertea M, Kim D, Pertea GM, Leek JT, Salzberg SL, 2016. Transcript-level expression analysis of RNA-seq experiments with HISAT, StringTie and Ballgown. Nature Protocols 11, 1650–1667. [PubMed: 27560171]

Probst FJ, Cooper ML, Cheung SW, Justice MJ, 2008. Genotype, phenotype, and karyotype correlation in the XO mouse model of Turner Syndrome. J Hered 99, 512–517. [PubMed: 18499648]

Richards MH, Seaton MS, Wallace J, Al-Harthi L, 2014. Porcupine Is Not Required for the Production of the Majority of Wnts from Primary Human Astrocytes and CD8+ T Cells. PLoS ONE 9, e92159. [PubMed: 24647048]

Robertson EJ, Norris DP, Brennan J, Bikoff EK, 2003. Control of early anterior-posterior patterning in the mouse embryo by TGF-β signalling. Philosophical Transactions of the Royal Society of London. Series B: Biological Sciences 358, 1351–1358.

Russell WL, Russell LB, Gower JS, 1959. Exceptional Inheritance of a Sex-Linked Gene in the Mouse Explained on the Basis That the X/O Sex-Chromosome Constitution Is Female. Proc Natl Acad Sci U S A 45, 554–560. [PubMed: 16590412]

Sato N, Meijer L, Skaltsounis L, Greengard P, Brivanlou AH, 2004. Maintenance of pluripotency in human and mouse embryonic stem cells through activation of Wnt signaling by a pharmacological GSK-3-specific inhibitor. Nat Med 10, 55–63. [PubMed: 14702635]

Schmittgen TD, Livak KJ, 2008. Analyzing real-time PCR data by the comparative C(T) method. Nat Protoc 3, 1101–1108. [PubMed: 18546601]

Soares M, Haraguchi S, Torres-Padilla M-E, Kalmar T, Carpenter L, Bell G, Morrison A, Ring C, Clarke N, Glover D, Zernicka-Goetz M, 2005. BMC Developmental Biology 5, 28. [PubMed: 16381610]

Stankova V, Tsikolia N, Viebahn C, 2015. Rho kinase activity controls directional cell movements during primitive streak formation in the rabbit embryo. Development 142, 92–98. [PubMed: 25516971]

Subramanian A, Tamayo P, Mootha VK, Mukherjee S, Ebert BL, Gillette MA, Paulovich A, Pomeroy SL, Golub TR, Lander ES, Mesirov JP, 2005. Gene set enrichment analysis: a knowledge-based approach for interpreting genome-wide expression profiles. Proc Natl Acad Sci U S A 102, 15545–15550. [PubMed: 16199517]

Sugawara A, Goto K, Sotomaru Y, Sofuni T, Ito T, 2006. Current status of chromosomal abnormalities in mouse embryonic stem cell lines used in Japan. Comp Med 56, 31–34. [PubMed: 16521857]

Takaoka K, Yamamoto M, Hamada H, 2011. Origin and role of distal visceral endoderm, a group of cells that determines anterior-posterior polarity of the mouse embryo. Nat Cell Biol 13, 743–752. [PubMed: 21623358]

Tao H, Suzuki M, Kiyonari H, Abe T, Sasaoka T, Ueno N, 2009. Mouse prickle1, the homolog of a PCP gene, is essential for epiblast apical-basal polarity. Proceedings of the National Academy of Sciences 106, 14426–14431.

ten Berge D, Koole W, Fuerer C, Fish M, Eroglu E, Nusse R, 2008. Wnt Signaling Mediates Self-Organization and Axis Formation in Embryoid Bodies. Cell Stem Cell 3, 508–518. [PubMed: 18983966]

Topol L, Jiang X, Choi H, Garrett-Beal L, Carolan PJ, Yang Y, 2003. Wnt-5a inhibits the canonical Wnt pathway by promoting GSK-3-independent beta-catenin degradation. J Cell Biol 162, 899–908. [PubMed: 12952940]

Trichas G, Joyce B, Crompton LA, Wilkins V, Clements M, Tada M, Rodriguez TA, Srinivas S, 2011. Nodal dependent differential localisation of dishevelled-2 demarcates regions of differing cell behaviour in the visceral endoderm. PLoS Biol 9, e1001019. [PubMed: 21364967]

Turner DA, Girgin M, Alonso-Crisostomo L, Trivedi V, Baillie-Johnson P, Glodowski CR, Hayward PC, Collignon J, Gustavsen C, Serup P, Steventon B, Lutolf MP, Arias AM, 2017. Anteroposterior polarity and elongation in the absence of extra-embryonic tissues and of spatially localised signalling in gastruloids: mammalian embryonic organoids. Development 144, 3894–3906. [PubMed: 28951435]

Vallier L, Reynolds D, Pedersen RA, 2004. Nodal inhibits differentiation of human embryonic stem cells along the neuroectodermal default pathway. Dev Biol 275, 403–421. [PubMed: 15501227]

Vallier L, Touboul T, Chng Z, Brimpari M, Hannan N, Millan E, Smithers LE, Trotter M, Rugg-Gunn P, Weber A, Pedersen RA, 2009. Early cell fate decisions of human embryonic stem cells and mouse epiblast stem cells are controlled by the same signalling pathways. PLoS One 4, e6082. [PubMed: 19564924]

van Amerongen R, Nusse R, 2009. Towards an integrated view of Wnt signaling in development. Development 136, 3205–3214. [PubMed: 19736321]

Vladar EK, Antic D, Axelrod JD, 2009. Planar Cell Polarity Signaling: The Developing Cell's Compass. Cold Spring Harbor Perspectives in Biology 1, a002964–a002964. [PubMed: 20066108]

Voiculescu O, Bertocchini F, Wolpert L, Keller RE, Stern CD, 2007. The amniote primitive streak is defined by epithelial cell intercalation before gastrulation. Nature 449, 1049–1052. [PubMed: 17928866]

Wallingford JB, Habas R, 2005. The developmental biology of Dishevelled: an enigmatic protein governing cell fate and cell polarity. Development 132, 4421–4436. [PubMed: 16192308]

Wang J, Hamblet NS, Mark S, Dickinson ME, Brinkman BC, Segil N, Fraser SE, Chen P, Wallingford JB, Wynshaw-Boris A, 2006. Dishevelled genes mediate a conserved mammalian PCP pathway to regulate convergent extension during neurulation. Development 133, 1767–1778. [PubMed: 16571627]

Wang J, Sinha T, Wynshaw-Boris A, 2012. Wnt Signaling in Mammalian Development: Lessons from Mouse Genetics. Cold Spring Harbor Perspectives in Biology 4, a007963–a007963. [PubMed: 22550229]

Willems E, Leyns L, Vandesompele J, 2008. Standardization of real-time PCR gene expression data from independent biological replicates. Anal Biochem 379, 127–129. [PubMed: 18485881]

Wray J, Kalkan T, Gomez-Lopez S, Eckardt D, Cook A, Kemler R, Smith A, 2011. Inhibition of glycogen synthase kinase-3 alleviates Tcf3 repression of the pluripotency network and increases embryonic stem cell resistance to differentiation. Nat Cell Biol 13, 838–845. [PubMed: 21685889]

Wynshaw-Boris A, 2012. Dishevelled, Planar Cell Polarity During Development. Elsevier, pp. 213–235.

Xu P, Davis RJ, 2010. c-Jun NH2-terminal kinase is required for lineage-specific differentiation but not stem cell self-renewal. Mol Cell Biol 30, 1329–1340. [PubMed: 20065035]

Xu Z, Robitaille AM, Berndt JD, Davidson KC, Fischer KA, Mathieu J, Potter JC, Ruohola-Baker H, Moon RT, 2016. Wnt/β-catenin signaling promotes self-renewal and inhibits the primed state transition in naïve human embryonic stem cells. Proceedings of the National Academy of Sciences 113, E6382–E6390.

Yamaguchi TP, Takada S, Yoshikawa Y, Wu N, McMahon AP, 1999. T (Brachyury) is a direct target of Wnt3a during paraxial mesoderm specification. Genes & Development 13, 3185–3190. [PubMed: 10617567]

Yamamoto M, Saijoh Y, Perea-Gomez A, Shawlot W, Behringer RR, Ang SL, Hamada H, Meno C, 2004. Nodal antagonists regulate formation of the anteroposterior axis of the mouse embryo. Nature 428, 387–392. [PubMed: 15004567]

Zhang M, Ngo J, Pirozzi F, Sun YP, Wynshaw-Boris A, 2018. Highly efficient methods to obtain homogeneous dorsal neural progenitor cells from human and mouse embryonic stem cells and induced pluripotent stem cells. Stem Cell Res Ther 9, 67. [PubMed: 29544541]

Zhao G-Q, 2002. Consequences of knocking out BMP signaling in the mouse. genesis 35, 43–56.

Highlights

- We investigated the role of the *Dishevelled* family of genes my making triple *Dvl1*, *Dvl2* and *Dvl3* null mutants (*Dvl* TKO).
- We identified several defects in anterior-posterior axis specification and mesoderm patterning in vivo
- We generated *Dvl* TKO mouse embryonic stem cells (mESCs) and compared the transcriptional profile of these cells with *wild-type* (*WT*) mESCs during germ lineage differentiation into 3D embryoid bodies (EBs).
- We identified major transcriptional dysregulation in the *Dvl* TKO EBs during differentiation in a number of genes involved in anterior-posterior pattern specification, gastrulation induction, mesenchyme morphogenesis, and mesoderm-derived tissue development.

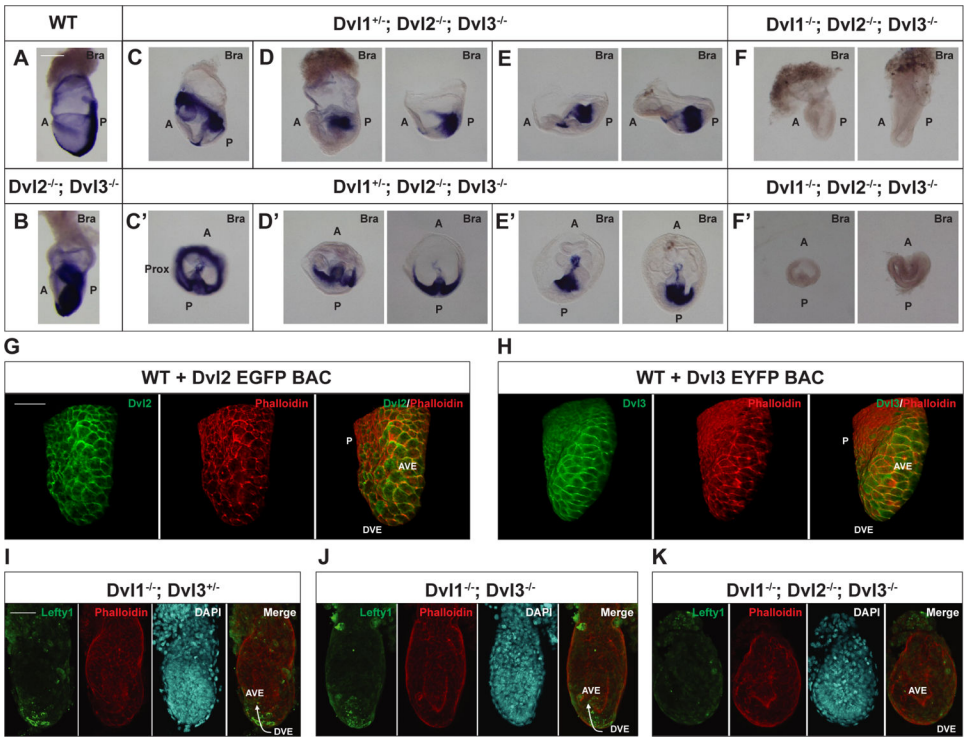

Figure 1. Loss of the *Dvls* Disrupts Anterior-Posterior Axis Specification and Mesoderm Patterning.

Whole-mount *in situ* hybridization staining for mesoderm marker, Brachyury, in representative E7.5 embryos. The expression patterns of Brachyury are shown for **A)** *WT* (n=1), **B)** *Dvl2*$^{-/-}$*; Dvl3*$^{-/-}$ (n=1), **C-E)** *Dvl1*$^{+/-}$*; Dvl2*$^{-/-}$*; Dvl3*$^{-/-}$ (n=5), and **F)** *Dvl1*$^{-/-}$*; Dvl2*$^{-/-}$*; Dvl3*$^{-/-}$ (n=2) embryos. **C–F)** Lateral and **C'-F')** transverse views of the egg cylinders are shown. **B)** *Dvl2*$^{-/-}$*; Dvl3*$^{-/-}$ embryos exhibit excessive accumulation of Brachyury-positive mesoderm in the posterior region, leading to the widespread appearance of expression throughout the embryo. *Dvl1*$^{+/-}$*; Dvl2*$^{-/-}$*; Dvl3*$^{-/-}$ display multiple developmental defects, including **C–C')** proximal Brachyury expression, **D–D')** accumulation of mesoderm in the proximal posterior region, and **E-E')** disorganization of the anterior ectoderm. **F-F')** *Dvl1*$^{-/-}$*; Dvl2*$^{-/-}$*; Dvl3*$^{-/-}$ embryos are smaller than the other *Dvl* mutants and completely lack Brachyury expression. **G-H)** Immunofluorescence staining of E6.5 transgenic embryos expressing *Dvl2-EGFP* and *Dvl3-EYFP* BAC transgenes show polarized expression of **G)** Dvl2-EGFP (green) (n=1) and **H)** Dvl3-EYFP (green) (n=1) in the DVE and AVE. Phalloidin (red) stains the actin filaments for contrast. **I-K)** To demonstrate DVE migration to the prospective anterior, immunofluorescence staining for Lefty1 in E6.5 *Dvl* mutants is shown. Lefty1 (green) is expressed in the migrating DVE of **I)** *Dvl1*$^{-/-}$*; Dvl3*$^{+/-}$ (n=1) and **J)** *Dvl1*$^{-/-}$*; Dvl3*$^{-/-}$ (n=1) embryos, but it is absent in **K)** *Dvl1*$^{-/-}$*; Dvl2*$^{-/-}$*; Dvl3*$^{-/-}$ (n=1) embryos. Arrow indicates the direction of migration towards the prospective anterior of the embryo. DAPI (cyan) and phalloidin (red) stain the nuclei and actin filaments, respectively, for contrast. Scale bar = 200 μm. A, anterior; P, posterior; Prox, proximal; DVE, distal visceral endoderm; AVE, anterior visceral endoderm.

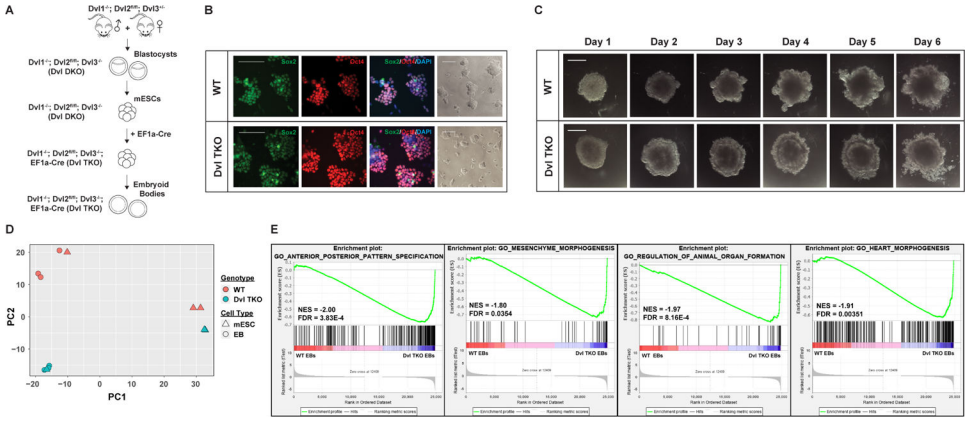

Figure 2: Generation of *Dvl* TKO Mouse Embryonic Stem Cells and Embryoid Bodies.

A) Schematic for the generation of *Dvl* TKO mESCs and EBs. Conditional $Dvl1^{-/-}$; $Dvl2^{flox/flox}$; $Dvl3^{-/-}$ blastocysts are isolated and cultured to generate mESCs, followed by transfection of EF1α-Cre recombinase to induce floxed *Dvl2* deletion. **B)** *WT* and *Dvl* TKO mESCs were stably passaged for more than 20 passages to confirm self-renewal properties (brightfield images) and stained for pluripotency markers, Sox2 (green), Oct4 (red), and nuclear DAPI (blue). Scale bars = 100 μm. **C)** Representative images of *WT* and *Dvl* TKO mESCs were differentiated into EBs over the time course of 6 days. Morphology of *Dvl* TKO EBs is distinct from *WT* EBs. An outer ectodermal ring of cells is visible in *Dvl* TKO EBs, but was not typically observed in *WT* EBs. Scale bar = 500 μm. **D)** Variance in global gene expression was compared between *WT* and *Dvl* TKO mESCs and EBs by principal component analysis. Among the *WT* and *Dvl* TKO mESCs an average absolute variance of 2.5% and 6.8% is observed along PC1 and PC2, respectively. One of the biological replicates for *WT* and *Dvl* TKO mESCs contained some differentiated cells, which led to clustering with the EBs. Otherwise, the mESCs displayed distinct separation from the differentiated EBs. There was a 31.3% variance between differentiating *WT* and *Dvl* TKO EBs along PC2. **E)** Genome-wide gene set enrichment analysis (GSEA) of genes in *WT* and *Dvl* TKO EBs. Significant enrichment of genes was observed in biological processes associated with axis specification, regulation of organ formation, and development of mesoderm-derived tissues, such as the mesenchyme and heart.

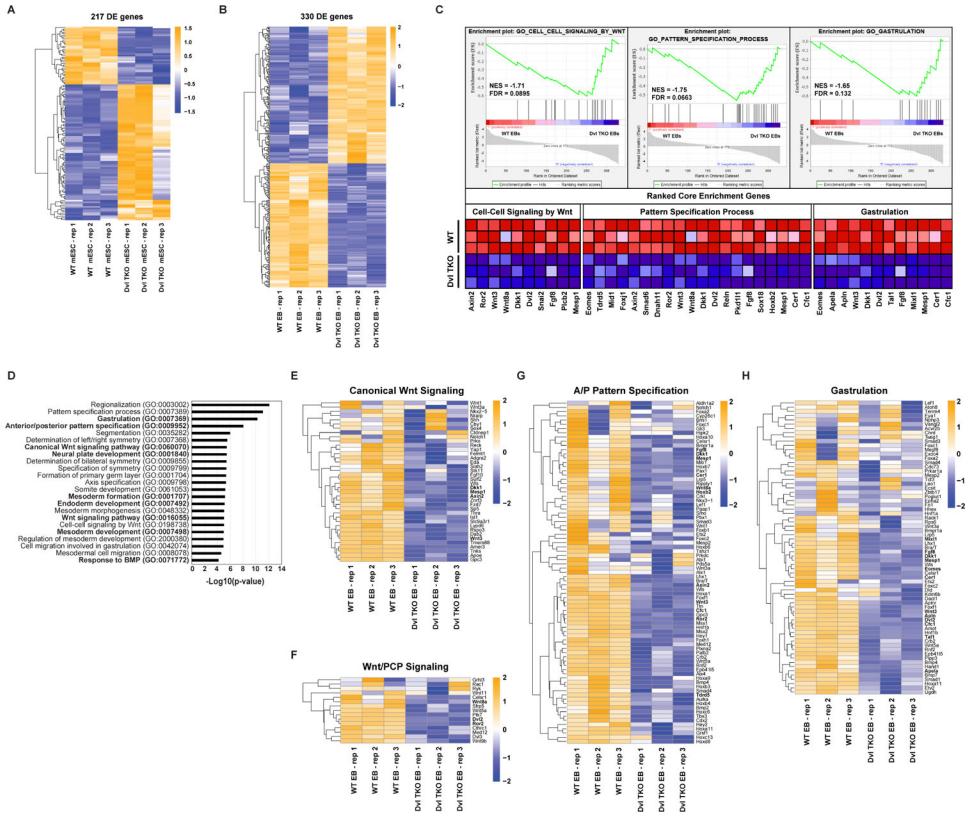

Figure 3: Identification of Gene Dysregulation in Developmental Processes and Pathways with *Dvl* Loss During Differentiation.

A) Heatmap of unsupervised hierarchical clustering of 217 significantly (FDR < 0.05) differentially expressed (DE) genes in biological triplicates of *WT* and *Dvl* TKO mESCs. **B)** Heatmap of unsupervised hierarchical clustering of 330 DE genes (FDR < 0.05) (173 up-regulated and 157 down-regulated in *Dvl* TKO EBs) in *WT* and *Dvl* TKO EBs during differentiation. **C)** Gene set enrichment analysis (GSEA) of 330 DE genes identified in *WT* and *Dvl* TKO EBs. Normalized Enrichment Score (NES) and FDR are shown for the top biological processes. The ranked core genes contributing to the NES are shown. **D)** Gene ontology (GO) analysis of the significantly 157 down-regulated genes in *Dvl* TKO EBs to identify the represented biological processes. **E-H)** Heatmaps of unsupervised hierarchical clustering of the relative gene expression of the specific GO terms highlighted in bold were further analyzed. The core GSEA genes are highlighted in bold in each of the following heatmaps. **E-F)** To infer canonical and non-canonical Wnt signaling functional activity, the gene expression levels of known regulatory and target genes were compared among *WT* and *Dvl* TKO EBs. **G-H)** In *Dvl* TKO EBs, significant down-regulation is observed in several genes involved in **G)** anterior-posterior pattern specification and **H)** gastrulation induction. All heatmap scales represent the Z-score of gene expression.

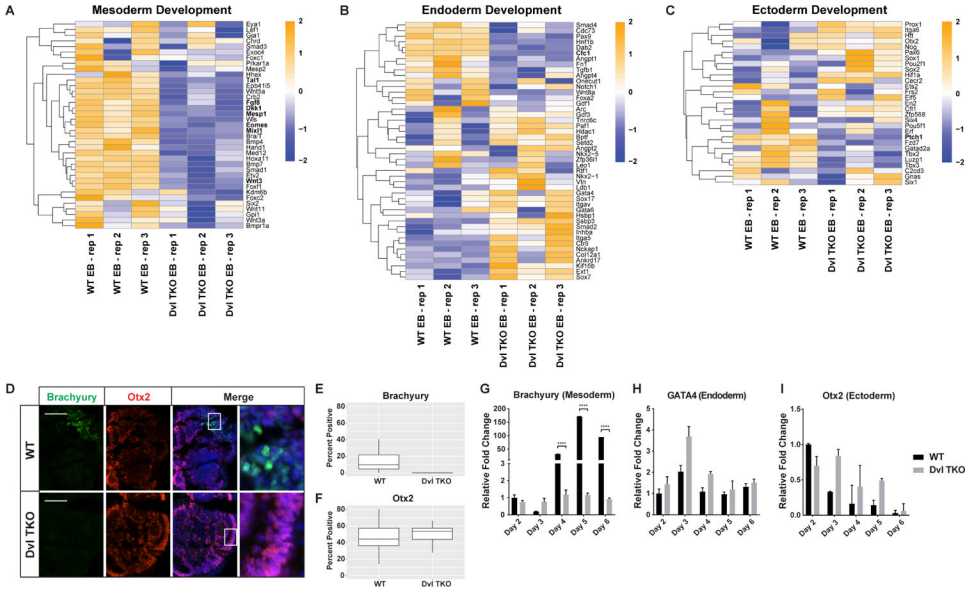

Figure 4: Loss of the *Dvls* Disrupts Mesoderm Differentiation but Endoderm and Ectoderm Induction Remain Intact.

A-C) Heatmaps of unsupervised hierarchical clustering of genes involved in germ lineage differentiation. **A)** In *Dvl* TKO EBs, significant down-regulation is observed in genes involved in mesoderm formation. Genes involved in **B)** endoderm and **C)** ectoderm formation are not exclusively down-regulated in *Dvl* TKO EBs, but display differential expression compared to *WT* EBs. All heatmap scales represent the Z-score of gene expression. **D)** Immunostaining of Brachyury (green), Otx2 (red), and DAPI (blue) in *WT* and *Dvl* TKO EBs at day 6. Mesodermal Brachyury-positive cells are undetectable in the *Dvl* TKO EBs. The outer ectodermal ring of cells that is present in *Dvl* TKO EBs, but not *WT* EBs, is positive for Otx2. Scale bar = 100 μm. **E-F)** Quantification of cells expressing Brachyury and Otx2 protein in *WT* and *Dvl* TKO EBs that were differentiated for 5–7 days (n=20/group). **G-I)** Expression levels of germ lineage markers Brachyury (mesoderm), GATA4 (endoderm), and Otx2 (ectoderm) were measured by qRT-PCR analysis (n=3). **G)** *WT* EBs display significant increases in Brachyury expression over time, whereas Brachyury levels in *Dvl* TKO EBs are at baseline throughout the differentiation process, indicating a lack of mesoderm differentiation in the absence of the *Dvls* that is consistent with defects observed *in vivo*. **H)** GATA4 (endoderm) expression is slightly higher in *Dvl* TKO EBs compared to *WT* throughout the course of differentiation, indicating that endoderm differentiation is not disrupted in the absence of the *Dvls*. However, these differences are not statistically significantly. **I)** The levels of Otx2 mRNA decline over time in *WT* EBs, but *Dvl* TKO EBs display a delay in decreased Otx2 expression and remain higher over the course of differentiation until day 6. *p < 0.05, **p < 0.01, ***p < 0.001, ****p < 0.0001.

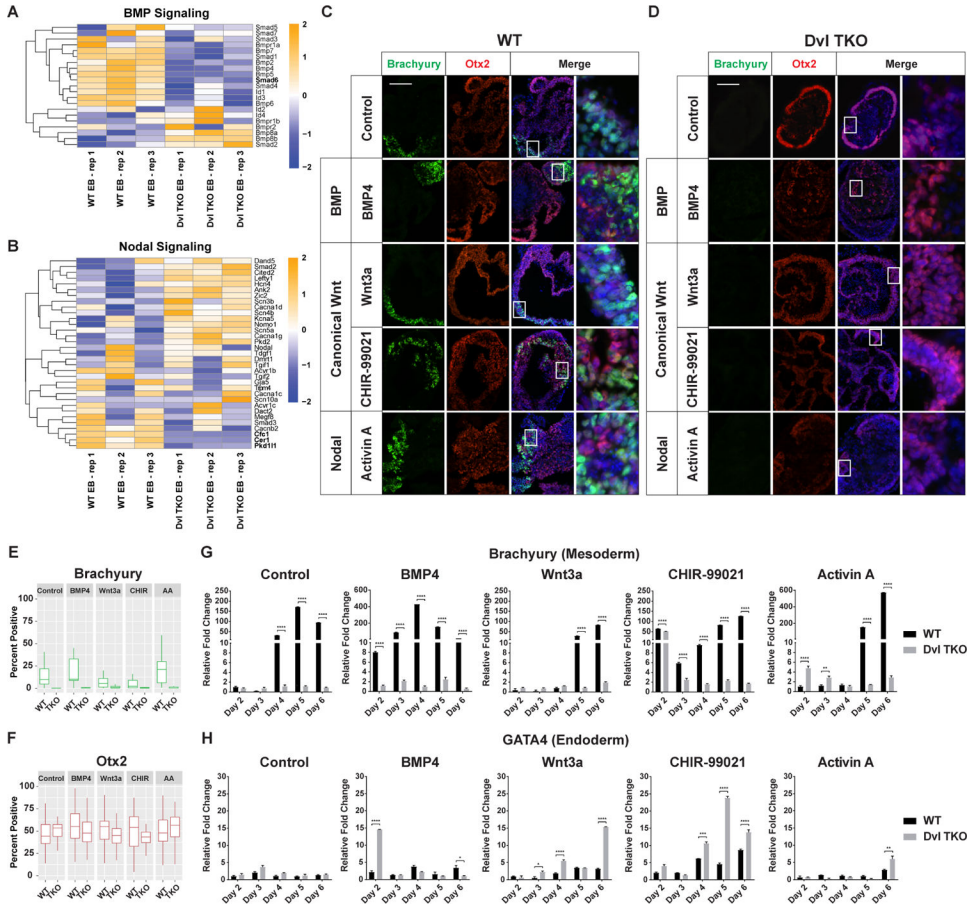

Figure 5: Effects of Activating BMP, Canonical Wnt, and Nodal signaling on Germ Lineage Differentiation.

A-B) Heatmaps of unsupervised hierarchical clustering of BMP and Nodal signaling genes. Many key BMP signaling genes were down-regulated in *Dvl* TKO EBs, whereas the pattern of expression for Nodal associated genes was not exclusively down in the *Dvl* TKO EBs, compared to *WT EBs*. All heatmap scales represent the Z-score of gene expression. **C-D)** Representative images of Brachyury (green), Otx2 (red), and DAPI (blue) immunostaining of *WT* and *Dvl* TKO EBs on day 7 of differentiation after activation with BMP (BMP4), canonical Wnt (Wnt3a and CHIR-99021) and Nodal (Activin A) drug treatments. Scale bar = 100 μm. **E-F)** Quantification of Brachyury and Otx2-positive cells in *WT* and *Dvl* EBs differentiated for 5–7 days (n=20/group). Brachyury-positive cells are not detectable in *Dvl* TKO EBs with activating drug treatments. There are no significant differences in Otx2-positive cells with activating drug treatments. **G-H)** Quantitative RT-PCR analysis of Brachyury (mesoderm) and GATA4 (endoderm) mRNA expression to determine differences in differentiation potential in *WT* and *Dvl* TKO EBs over a 6-day time course (n=3). **G)** Treatment with BMP4 and CHIR-99021 induced earlier expression of Brachyury in *WT* EBs compared to the untreated control suggesting that Wnt signaling may regulate timing and drive mesoderm induction. Wnt activation by Wnt3a and CHIR-99021 did not increase the overall levels of Brachyury in *WT* EBs relative to the untreated controls. Wnt3a, a negative control of Wnt activation upstream of the Dvls, did not induce mesoderm differentiation in

Dvl TKO EBs. Only direct exposure to CHIR-99021 in *Dvl* TKO EBs (Day 2) resulted in Brachyury expression, but was not maintained over time. BMP4 and Activin A led to more robust increases in Brachyury compared to Wnt activation in *WT* EBs but did not rescue expression in *Dvl* TKO EBs. **H)** The relative levels of GATA4 is higher in *Dvl* TKO EBs compared to *WT* EBs in the control and with treatment. The absence of mesoderm differentiation may contribute to increased endoderm induction in the *Dvl* TKO EBs.

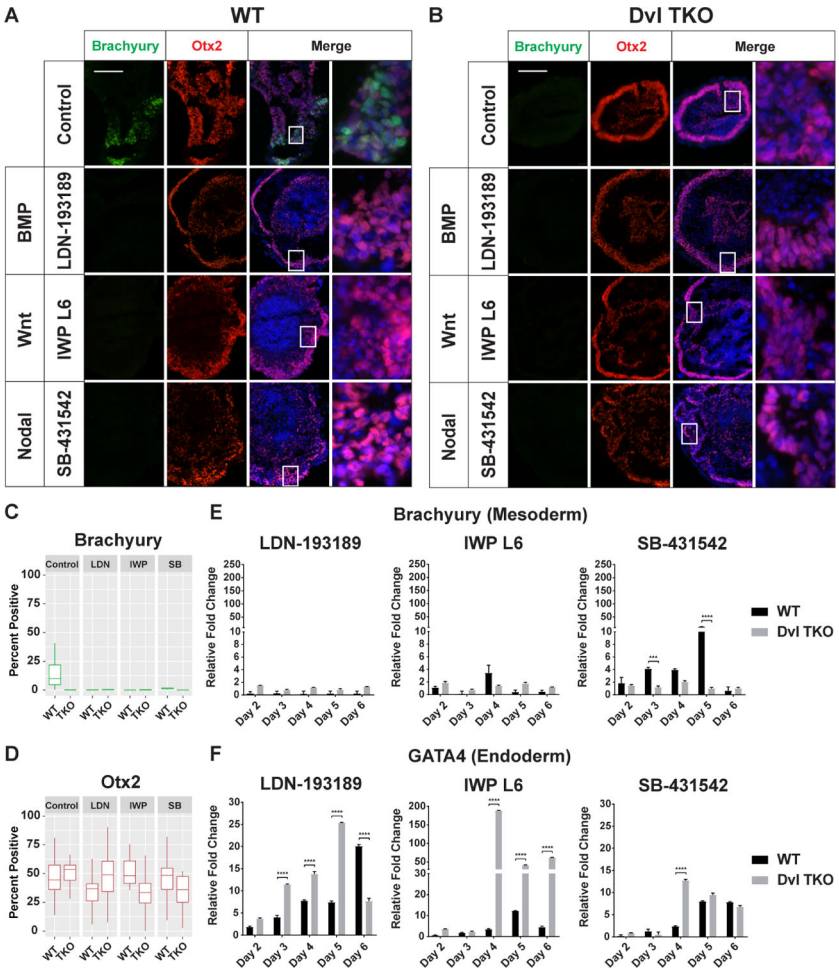

Figure 6: Effects of Inhibiting BMP, Canonical Wnt, and Nodal signaling on Germ Lineage Differentiation.

A-B) Representative images of Brachyury (green), Otx2 (red), and DAPI (blue) immunostaining of *WT* and *Dvl* TKO EBs on day 7 of differentiation after inhibition with BMP (LDN-193189), canonical and non-canonical Wnt (IWP L6) and Nodal (SB-431542) drug treatments. Scale bar = 100 μm. **C-D)** Quantification of Brachyury and Otx2-positive cells in *WT* and *Dvl* EBs differentiated for 5–7 days (n=20/group). Brachyury-positive cells are not detectable in *Dvl* TKO EBs, and there are no significant differences in Otx2-positive cells. **E-F)** Quantitative RT-PCR analysis of Brachyury (mesoderm) and GATA4 (endoderm) mRNA expression to determine differences in differentiation potential in *WT* and *Dvl* TKO EBs over a 6-day time course (n=3). Expression is normalized to the untreated controls in Figure 5G (Brachyury) and 5H (GATA4). **E)** Brachyury expression in *WT* EBs is attenuated with inhibition of BMP, Wnt, and Nodal signaling, similar to *Dvl* TKO EBs. **F)** Inhibition of BMP and Wnt signaling significantly enhances endoderm differentiation in *WT* and *Dvl* TKO EBs. *p < 0.05, **p < 0.01, ***p < 0.001, ****p < 0.0001.

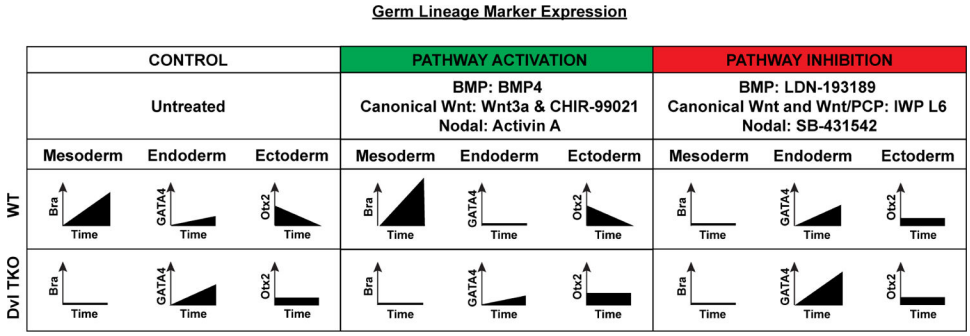

Figure 7: Effects of Developmental Pathway Modulation on Germ Lineage Differentiation.

Activation of BMP (BMP4), canonical Wnt (Wnt3a and CHIR-99021) and Nodal (Activin A) pathways in *WT* EBs enhances mesoderm (Bra) differentiation, while endoderm (GATA4) differentiation remains low, and ectoderm (Otx2) differentiation diminishes over time. Treatment with these activators in *Dvl* TKO EBs does not rescue mesoderm induction. The relative level of endoderm marker expression is higher in *Dvl* TKO EBs compared to *WT* EBs treated with Wnt activators, Wnt3a and CHIR, but not BMP4 or Activin A. *Dvl* loss also delays the decrease in ectoderm lineage expression. Inhibition of BMP (LDN-198189), canonical and non-canonical Wnt (IWP L6) and Nodal (SB431542) pathways in *WT* EBs results in the suppression of mesoderm differentiation, recapitulating the *Dvl* TKO phenotype. Pathway inhibitor treatment in *WT* EBs, leads to similar trends of differentiation as *Dvl* TKO EBs. Endoderm differentiation is greatly enhanced in *Dvl* TKO EBs with LDN-193189 and IWP L6 treatment.